AJCMI
Avicenna Journal of Clinical Microbiology and Infection
Avicenna J Clin Microbiol Infect. 2025;12(3):139-S1. doi:10.34172/ajcmi.3692
http://ajcmi.umsha.ac.ir

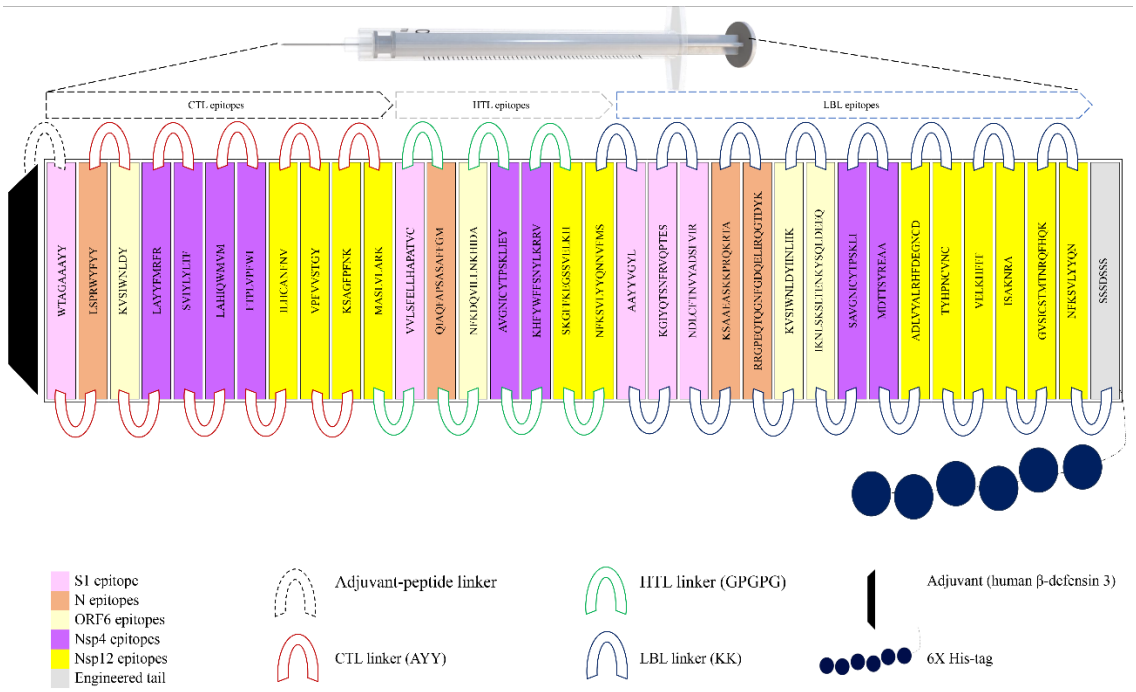

Figure S1. Arrangement of final anti-SARS-CoV-2 MEV with its various components

Table S1. Physicochemical properties of final construct

Parameter	Predicted value
Number of amino acids	571
Molecular weight	65440.68 Da
Formula	$C_{3013}H_{4563}N_{797}O_{795}S_{24}$
Theoretical isoelectric point (pI)	9.79
Total number of negatively charged residues (Asp + Glu)	31
Total number of positively charged residues (Arg + Lys)	92
Half-life	30 hours (mammalian reticulocytes, in vitro). >20 hours (yeast, *in-vivo*) >10 hours (Escherichia coli, *in-vivo*)
Instability index (II)	34.80 (stable)
Aliphatic index	65.46
Grand average of hydropathicity (GRAVY)	-0.478

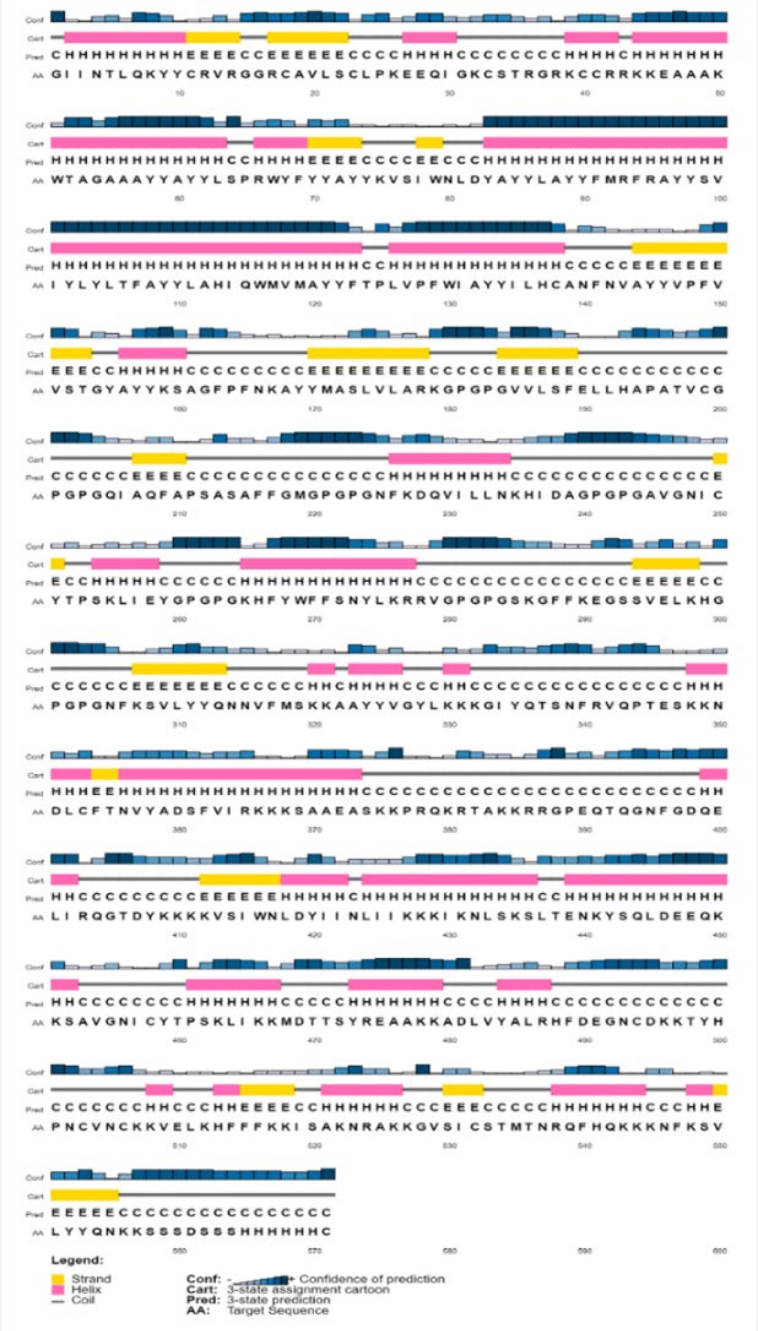

Figure S2. Prediction of possible 2D structure of anti-SARS-CoV-2 MEV using PSIPRED server

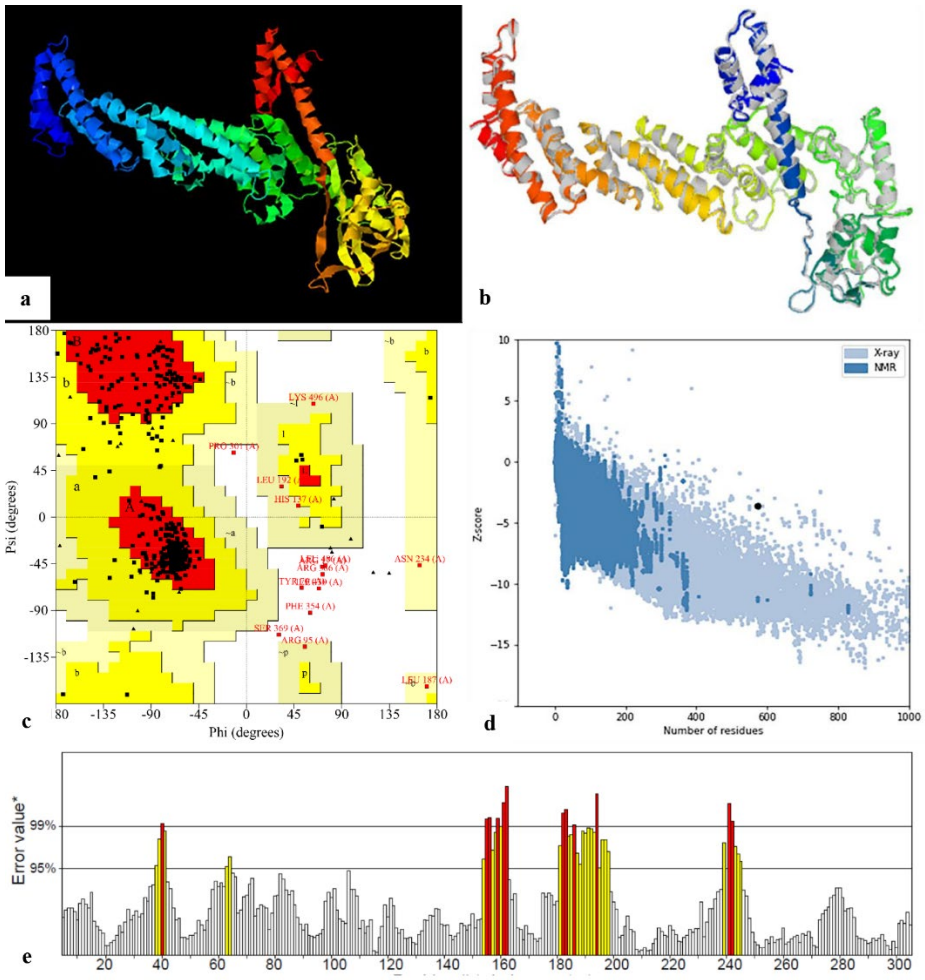

Figure S3. Modeling, refinement and validation of 3D structure of MEV. **(a)** the modelled structure by I-TASSER; **(b)** the selected refined model by GalaxyRefine server; **(c)** Ramachandran plot analysis by PROCHECK tool; the quality assessment of the MEV model by **(d)** the z-score plot; and **(e)** ERRAT tool, respectively

Table S2. Predicted conformational epitopes in the vaccine construct

No.	Residues	Number of residues	Score
1	A521, R524, A525, K526, K527, G528, V529, S530, I531, C532, S533, T534, M535, T536, N537, R538, F540, H541, Q542, K545, N546, F547, K548, S549, V550, L551, Y552, Y553, Q554, N555, K557, S558, S559, S560, D561, S562, S563, S564, H565, H566, H567, H568, H569, H570, C571	45	0.78
2	G1, I2, I3, N4, T5, L6, Q7, K8, Y9, Y10, C11, R12, V13, R14, G15, G16, R17, C18, A19, V20, L21, S22, C23, L24, P25, K26, E27, E28, Q29, I30, G31, K32, C33, S34, T35, R36, G37, R38, K39, C40, C41, R42, R43, K44, K45, E46, A47, A48, A49, K50, W51, T52, A53, G54, A55, A56, A57, Y58, Y59, A60, Y61, Y62, L63, S64, P65, R66, Y68, F69, Y70, Y71, A72, Y73, K75, V76, S77, I78, W79, N80, L81, D82, Y83, A84, Y85, Y86, L87, A88, Y89, Y90, F91, M92, R93, F94, R95, A96, Y97, Y98, V100, I101, Y102, L105, T106	101	0.768
3	F362, R365, I402, R403, Q404, G405, T406, D407, Y408, K409, K410, K411, K412, N423, L424, I425, I426, K427, K428, K429, I430, K431, N432, L433, S434, K435, S436, L437, T438, E439, N440, K441, Y442, S443, Q444, L445, D446, E447, K450, K451, V454, C458, Y459, T460, P461, S462, K463, L464, I465, K466, K467, M468, D469, T470, T471, S472, R474, E475, A476, A477, K478, K479, A480, D481, L482, V483, Y484, A485, L486, R487, H488, F489, D490, E491, G492, N493, C494, D495, K496, K497, T498	81	0.716
4	N315, M318, S319, K321, A322, A323, Y324, Y325, V326, G327, Y328, L329, K330, K331, G333, I334, Y335, Q336, T337, S338, N339, F340, R341, V342, Q343, P344, I364, K366, K367, K368, S369, A370, A371, E372, A373, S374, K375, K376, P377, R378, Q379, K380, R381, T382, A383, K384, K385, R386, G388, P389, E390, Q391, T392	53	0.644
5	Y499, H500, P501	3	0.544

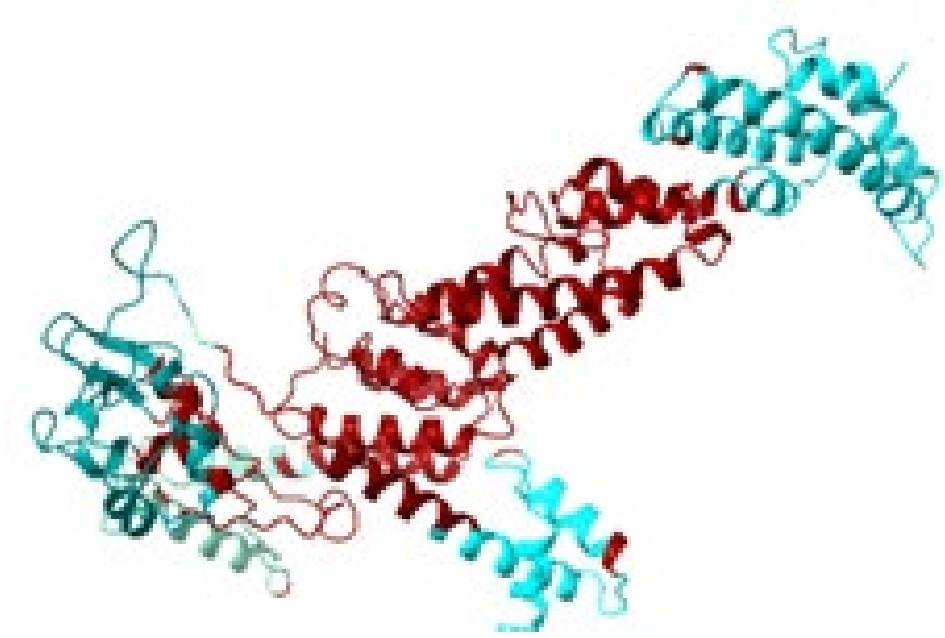

Figure S4. Topology of predicted conformational BCEs in anti-SARS-CoV-2 MEV (in the various ranges of cyan). Non-epitope parts remained in the dark red.

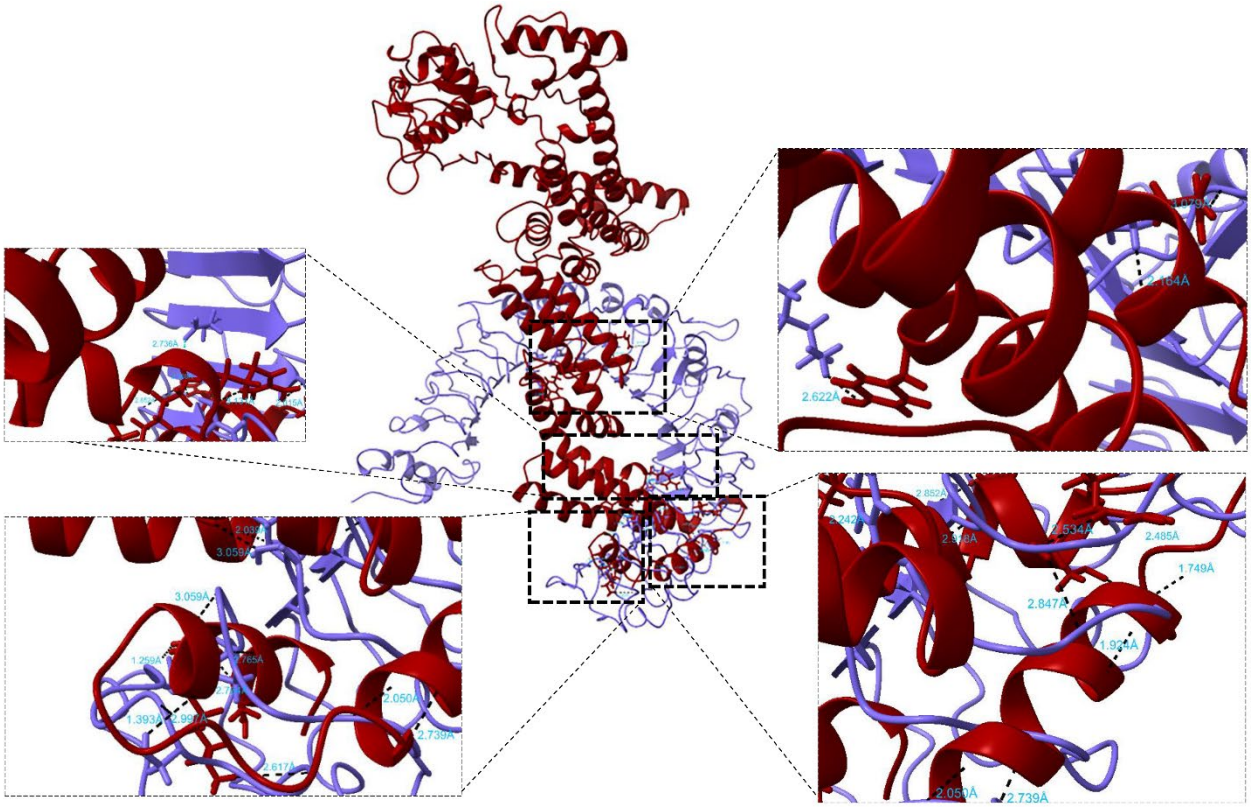

Figure S5. Analysis of molecular docking between TLR4-anti-SARS-CoV-2 MEV in docked complex using UCSF ChimeraX [Vaccine construct in dark red, TLR4 in purple, salt bridges and hydrogen bonds are displayed in cyan and black, respectively].

Table S3. Analysis of possible H-bonds and salt-bridges via molecular docking between TLR4-anti-SARS-CoV-2-MEV in docked complex

TLR4		MEV		D-H…A Distance (Å)	H-bond type according to (34)
Residue No.	**Atom name**	**Residue No.**	**Atom name**		
SER207	OG	**ARG93**	NH1	1.207	Very strong
LEU208	O	**ARG38**	NE	3.225	Weak
ASP209 (Hbond and salt bridge)	OD2	**ARG95**	NH1	2.547	Strong
ASP209 (Hbond and salt bridge)	OD2	**ARG95**	NH2	2.119	Very strong
LEU210	N	**GLU28**	OE1	2.946	Strong
ASN213	O	**LYS39**	N	2.723	Strong
LEU231	N	**TYR90**	O	2.985	Strong
LEU231	N	**PHE91**	O	2.908	Strong
THR232	OG1	**GLU46**	OE2	3.188	Weak
ASN236	ND2	**GLU27**	O	2.127	Very strong
ILE247	O	**GLN29**	NE2	2.234	Very strong
HIS256	ND1	**ARG17**	NE	2.888	Strong
ARG257	NH2	**ALA49**	O	3.286	Weak
ARG257	NE	**MET92**	O	2.366	Very strong
GLY261	N	**GLU27**	OE1	2.080	Very strong
ARG289	NE	**THR52**	OG1	1.354	Very strong
PHE313	O	**GLN7**	H	0.912	Very strong
PHE313	O	**LYS8**	N	2.979	Strong
SER314	N	**ILE2**	O	1.350	Very strong
HIS334	ND1	**LEU6**	O	0.850	Very strong
GLU336	N	**ILE3**	O	2.523	Strong
GLU336	OE2	**ALA56**	N	2.682	Strong
THR357	N	**GLN7**	OE1	3.060	Strong
LEU404	O	**ARG66**	NH1	3.043	Strong
SER407	N	**TYR62**	OH	2.496	Very strong

[a] D-H..A dist.: Hydrogen (H) of donor (D)-acceptor (A) distance

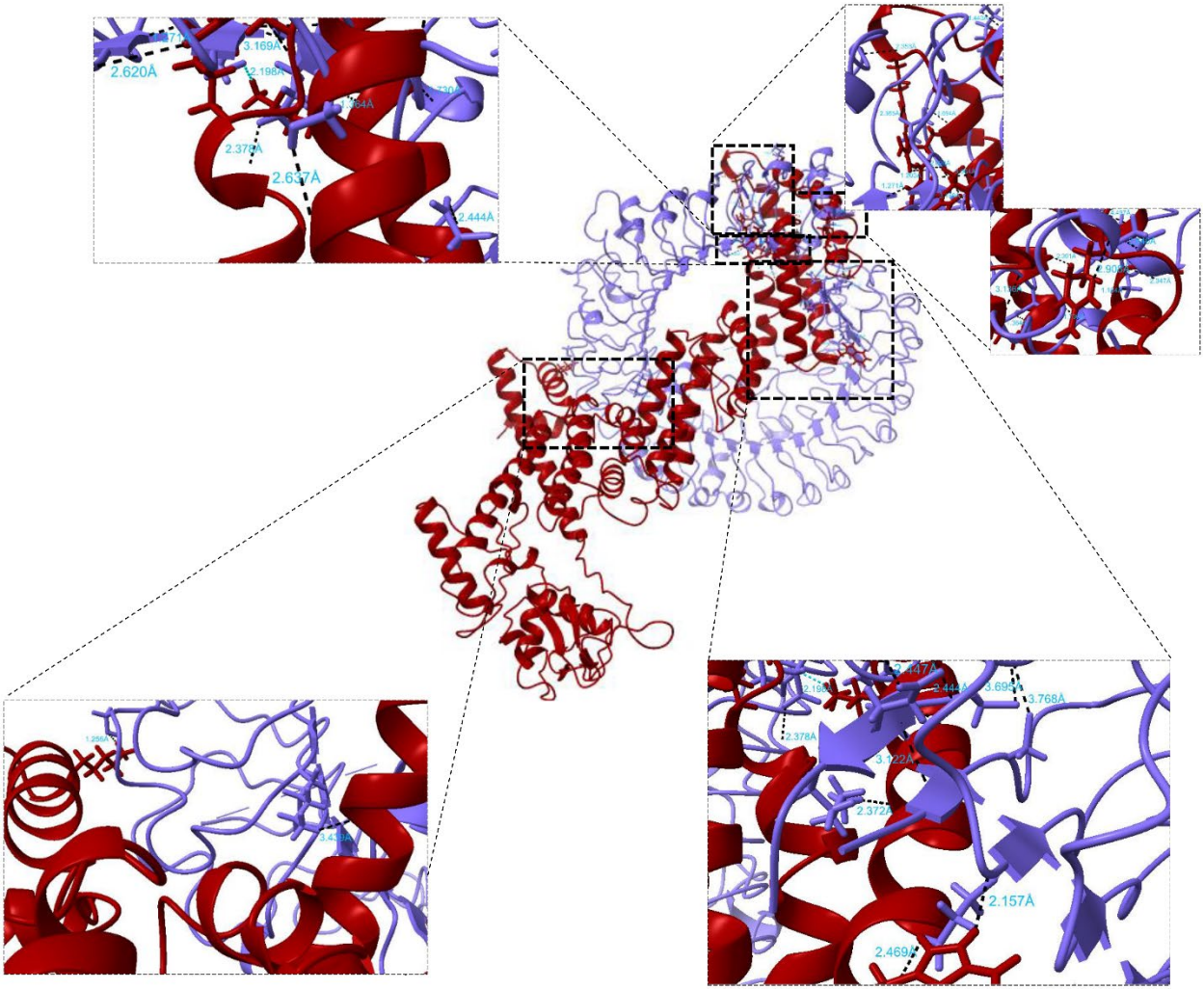

Figure S6. Analysis of molecular docking between TLR8-anti-SARS-CoV-2 MEV in docked complex using UCSF ChimeraX [Vaccine construct in dark red, TLR8 in purple, salt bridges and hydrogen bonds are displayed in cyan and black, respectively].

Table S4. Analysis of possible H-bonds and salt-bridges via molecular docking between TLR8-anti-SARS-CoV-2-MEV in docked complex

Residue No.	Atom name	Residue No.	Atom name	D-H…A Distance (Å)	H-bond type (34)
TLR8		MEV			
CYS36	O	**CYS11**	SG	3.084	Strong
ASP37	OD1	**ALA56**	N	2.444	Very strong
ASP37	O	**ALA60**	N	3.122	Weak
GLU38	OE1	**ARG12**	N	2.447	Very strong
LYS39	NZ	**ALA57**	O	2.372	Very strong
THR66	O	**TRP67**	NE1	2.157	Very strong
GLU67	OE1	**ARG66**	N	2.469	Very strong
SER522	OG	**LYS544**	NZ	1.256	Very strong
LYS533	NZ	**SER212**	O	3.439	Weak
LEU701	O	**GLY37**	N	2.353	Very strong
ARG715	O	**ARG93**	NH2	2.620	Strong

LEU717	O	**ARG95**	NE	1.271	Very strong
ASP742	O	**ARG42**	NH1	1.203	Very strong
ASP742 (Hbond and salt bridge)	OD1	**LYS50**	NZ	2.198	Very strong
LEU743	N	**ARG93**	O	3.169	Weak
SER744	O	**ARG42**	NH1	2.624	Strong
ASN746	OD1	**ARG36**	NE	2.385	Very strong
ASN746	O	**ARG43**	N	1.694	Very strong
LYS749	NZ	**GLN29**	O	1.443	Very strong
SER765	OG	**LEU81**	O	2.637	Strong
GLU768	O	**ARG95**	NH1	3.064	Strong
GLU768	OE2	**TYR97**	N	2.378	Very strong
HIS770	ND1	**LYS50**	N	1.364	Very strong
ASP788	O	**ARG17**	NH1	2.908	Strong
ASP788	OD1	**VAL20**	N	2.640	Strong
VAL793	O	**PHE91**	N	3.136	Weak
ASP800	N	**ALA48**	O	1.730	Very strong
ILE802	N	**LYS44**	O	2.391	Very strong
SER813	O	**GLY1**	N	2.347	Very strong
SER813	OG	**ILE3**	N	1.184	Very strong

[a] D-H..A dist.: Hydrogen (H) of donor (D)-acceptor (A) distance

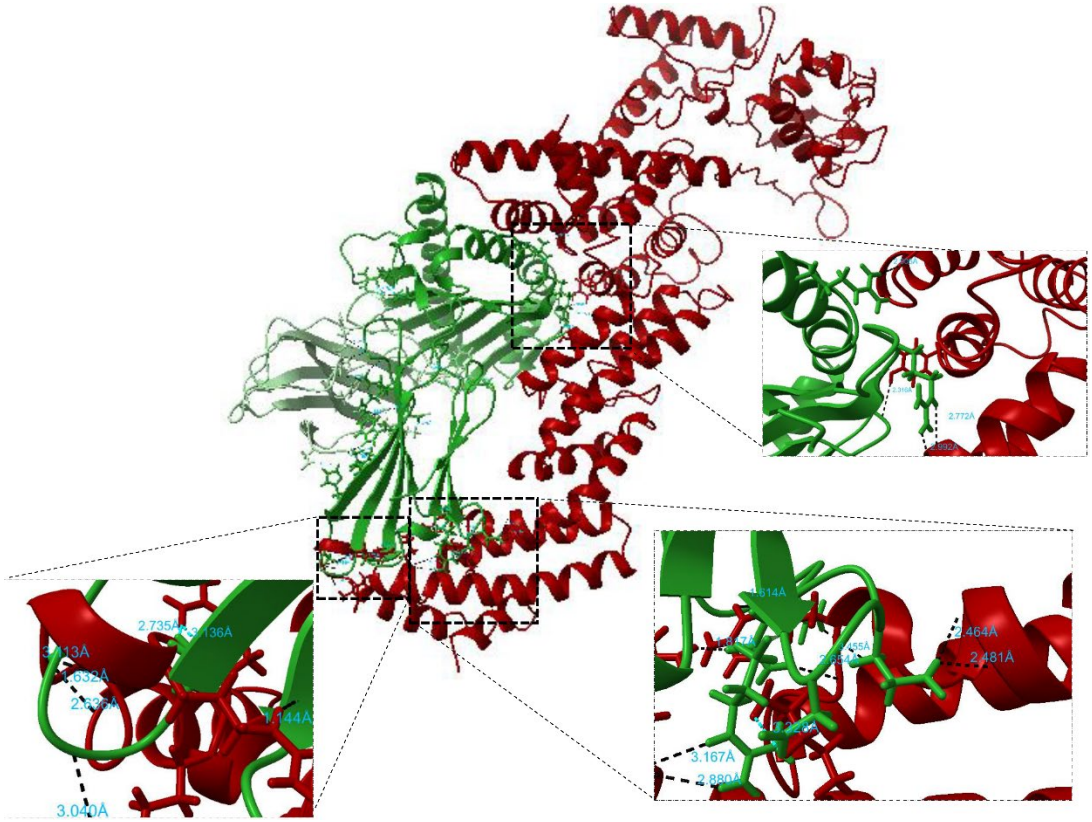

Figure. S7. Analysis of molecular docking between HLA-A*03:01-anti-SARS-CoV-2 MEV in docked complex using UCSF ChimeraX [Vaccine construct in dark red, A chain of HLA-A*03:01 in dark green, β_2-microglubolin in light green; salt bridges and hydrogen bonds are displayed in cyan and black, respectively].

Table S5. Analysis of possible H-bonds and salt-bridges via molecular docking between HLA-A*03:01-anti-SARS-CoV-2-MEV in docked complex

Residue No.	Atom name	Residue No.	Atom name	D-H…A Distance (Å)	H-bond type (34)[47]
HLA-A*03:01		MEV			
ARG108	NE	**PRO211**	O	2.772	Strong
ARG108	NH2	**SER212**	OG	2.992	Strong
ASP129	O	**TYR251**	OH	2.316	Very strong
ARG169	NH2	**PRO301**	O	2.906	Strong
SER195	OG	**ARG36**	N	1.632	Very strong
ASP196	O	**LYS39**	NZ	3.040	Strong
HIS197	N	**CYS33**	O	2.636	Strong
GLU198	N	**CYS33**	O	3.113	Weak
GLU198 (Hbond and salt bridge)	OE1	**ARG38**	NH1	2.735	Strong
GLU198 (Hbond and salt bridge)	OE2	**ARG38**	NH1	3.136	Weak
ARG219	NE	**ARG42**	O	3.167	Weak
ARG219	NH1	**ARG42**	O	2.880	Strong
ASP220 (Hbond and salt bridge)	OD2	**LYS50**	NZ	3.328	Weak
GLU222	OE1	**VAL100**	N	2.464	Very strong
GLU222	OE1	**ILE101**	N	2.481	Very strong
GLN224	OE1	**ARG42**	NH1	1.817	Very strong
GLN224	NE2	**PHE94**	O	2.654	Strong
GLN226	NE2	**TYR85**	O	3.455	Weak
GLN226	O	**ARG95**	NE	1.614	Very strong
VAL249	O	**ARG36**	NE	1.144	Very strong

[a] D-H..A dist.: Hydrogen (H) of donor (D)-acceptor (A) distance

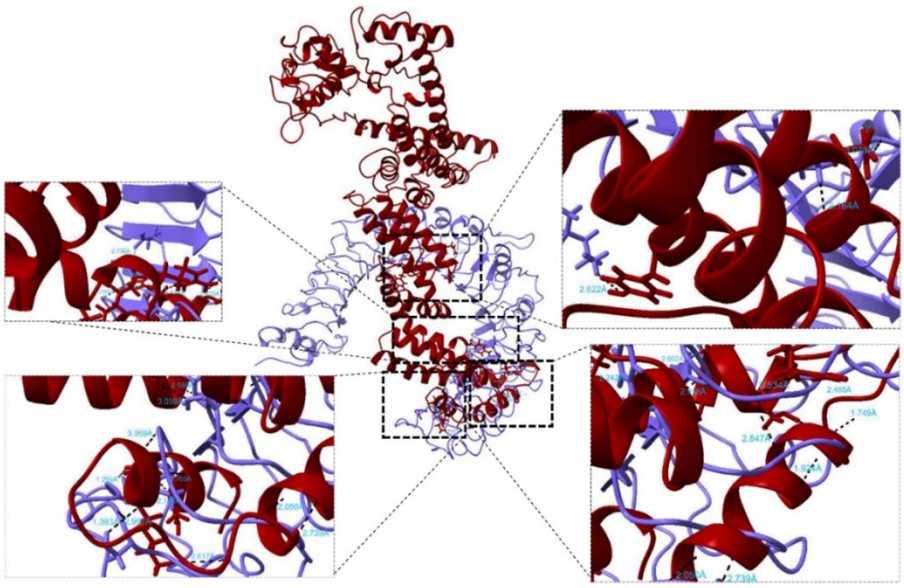

Figure S8. Analysis of molecular docking between TLR2-anti-SARS-CoV-2 MEV in docked complex using UCSF ChimeraX [Vaccine construct in dark red, TLR2 in purple, salt bridges and hydrogen bonds are displayed in cyan and black, respectively].

Table S6. Analysis of possible H-bonds and salt-bridges via molecular docking between TLR2-anti-SARS-CoV-2-MEV in docked complex

Residue No.	Atom name	Residue No.	Atom name	D-H…A Distance (Å)	H-bond type according to (34)
TLR2		MEV			
GLY38	N	**GLN7**	OE1	1.259	Very strong
GLY41	O	**ARG14**	N	1.393	Very strong
SER42	OG	**LYS8**	O	2.997	Strong
SER45	O	**LYS8**	NZ	2.617	Strong
ASP58	N	**ASN4**	OD1	2.765	Strong
SER60	O	**TYR10**	N	3.059	Weak
ASN62	ND2	**ILE3**	O	2.764	Strong
ILE64	O	**LEU21**	N	2.050	Strong
THR84	OG1	**ALA53**	N	2.039	Very strong
SER85	OG	**TYR98**	OH	3.059	Strong
ASN89	N	**CYS18**	O	2.739	Strong
ASP106	OD2	**TRP51**	N	2.242	Very strong
TYR109	OH	**ARG95**	NH1	3.131	Weak
LEU112	O	**CYS41**	SG	2.847	Strong
ASN114	N	**PRO25**	O	1.924	Very strong
LEU115	O	**LYS32**	N	1.749	Very strong
SER116	O	**CYS40**	SG	2.485	Very strong
THR127	O	**ARG43**	NH2	2.852	Strong
ASN130	O	**ALA48**	N	2.918	Strong
ASN134	O	**ARG38**	NE	2.534	Strong
ILE139	O	**GLN208**	NE2	3.079	Strong
ILE153	O	**ARG43**	NE	2.368	Very strong
GLY157	O	**ARG95**	NH2	2.015	Very strong
GLU180 (Hbond and salt bridge)	OE2	**LYS50**	NZ	2.736	Strong
LYS347	NZ	**GLN205**	O	2.164	Very strong
LYS422	NZ	**TYR145**	OH	2.622	Strong

[a] D-H..A dist.: Hydrogen (H) of donor (D)-acceptor (A) distance

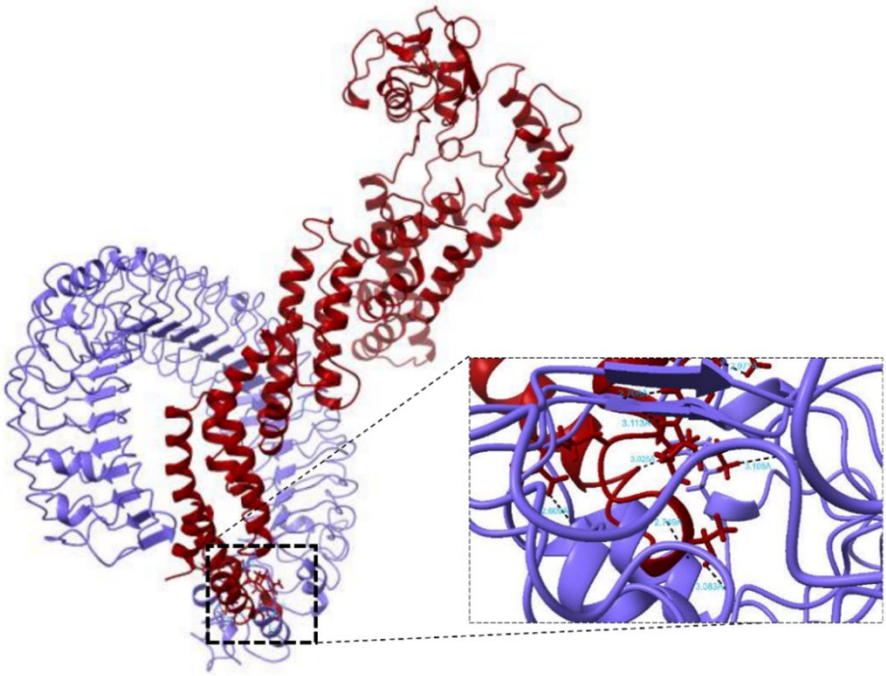

Figure S9. Analysis of molecular docking between TLR3-anti-SARS-CoV-2 MEV in docked complex using UCSF ChimeraX [Vaccine construct in dark red, TLR3 in purple, salt bridges and hydrogen bonds are displayed in cyan and black, respectively].

Table S7. Analysis of possible H-bonds and salt-bridges via molecular docking between TLR3-anti-SARS-CoV-2-MEV in docked complex

TLR3		MEV		D-H…A Distance (Å)	H-bond type according to (34)
Residue No.	**Atom name**	**Residue No.**	**Atom name**		
ILE654	O	**THR35**	OG1	3.083	Strong
PHE657	O	**ARG36**	N	2.749	Strong
GLU663	O	**ARG38**	NH1	2.609	Strong
ASN667	O	**ARG36**	NE	3.113	Weak
ASN667	O	**ARG36**	NH2	2.708	Strong
PRO669	O	**ARG43**	NH1	2.971	Strong
TYR675	O	**LYS39**	NZ	3.108	Weak
ARG689	NE	**ILE30**	O	3.025	Strong

[a] D-H..A dist.: Hydrogen (H) of donor (D)-acceptor (A) distance

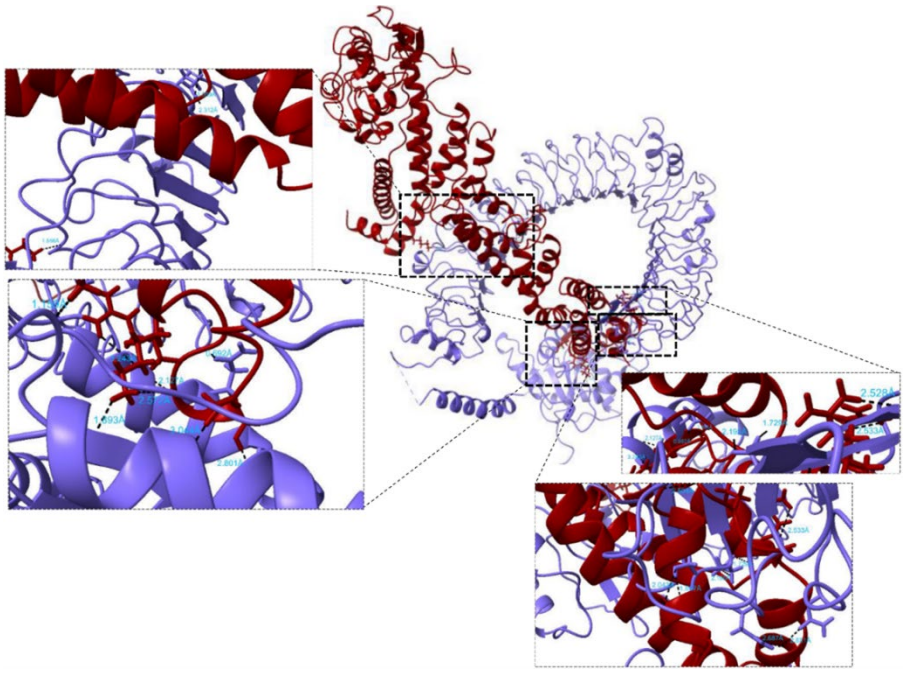

Figure S10. Analysis of molecular docking between TLR5-anti-SARS-CoV-2 MEV in docked complex using UCSF ChimeraX [Vaccine construct in dark red, TLR5 in purple, salt bridges and hydrogen bonds are displayed in cyan and black, respectively].

Table S8. Analysis of possible H-bonds and salt-bridges via molecular docking between TLR5-anti-SARS-CoV-2-MEV in docked complex

Residue No.	Atom name	Residue No.	Atom name	D-H…A Distance (Å)	H-bond type according to (34)
TLR5		MEV			
LEU45	O	**LYS8**	N	2.043	Very strong
THR48	OG1	**ASN4**	O	1.657	Very strong
GLU49	OE1	**PHE91**	N	1.729	Very strong
GLU49	OE2	**MET92**	N	2.195	Very strong
LEU52	N	**CYS11**	O	2.504	Strong
GLN71	OE1	**CYS23**	N	2.687	Strong
GLN73	O	**ARG17**	NH1	2.533	Strong
GLU76	O	**ARG14**	NH1	2.528	Strong
ASN96	OD1	**CYS23**	N	2.881	Strong
GLU432	OE2	**GLY204**	N	2.312	Very strong
GLN457	NE2	**GLY202**	O	3.059	Strong
TRP489	O	**LYS548**	NZ	1.556	Very strong
LYS692	O	**LYS44**	NZ	1.159	Very strong
ALA695	O	**LYS39**	NZ	1.893	Very strong
LEU697	O	**CYS33**	SG	3.044	Strong
ASP703	O	**SER34**	OG	2.801	Strong
GLN708	OE1	**GLY37**	N	0.692	Very strong
LEU712	O	**ARG36**	NH1	3.243	Weak
LYS713	N	**THR35**	O	2.127	Very strong
CYS728	O	**LYS39**	NZ	2.572	Strong

[a] D-H..A dist.: Hydrogen (H) of donor (D)-acceptor (A) distance

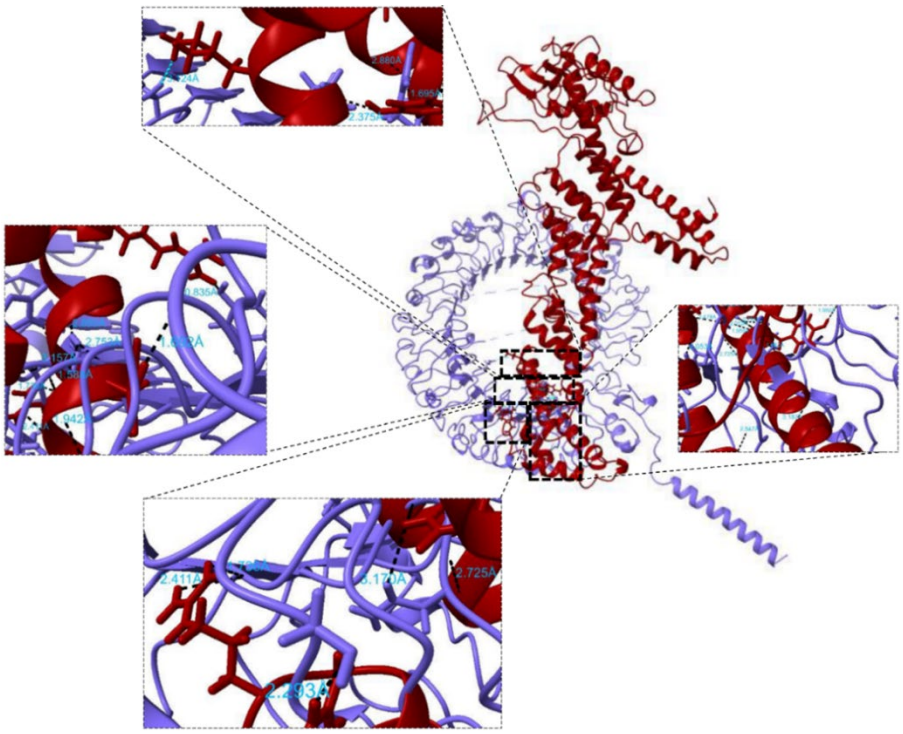

Figure S11. Analysis of molecular docking between TLR7-anti-SARS-CoV-2 MEV in docked complex using UCSF ChimeraX [Vaccine construct in dark red, TLR7 in purple, salt bridges and hydrogen bonds are displayed in cyan and black, respectively].

Table S9. Analysis of possible H-bonds and salt-bridges via molecular docking between TLR7-anti-SARS-CoV-2-MEV in docked complex

Residue No.	Atom name	Residue No.	Atom name	D-H…A Distance (Å)	H-bond type according to (34)
TLR7		MEV			
ASP605 (Hbond and salt bridge)	OD2	**LYS75**	NZ	3.124	Weak
SER661	OG	**ARG14**	NH1	2.293	Very strong
SER681	O	**ARG12**	NH1	1.736	Very strong
SER681	O	**ARG12**	NH2	2.411	Very strong
LYS684	NZ	**TYR102**	OH	2.375	Very strong
LYS688	NZ	**ALA84**	O	2.053	Very strong
SER707	OG	**ALA57**	O	3.157	Weak
SER707	OG	**TYR58**	O	2.753	Strong
SER707	OG	**SER64**	N	2.880	Strong
SER707	O	**ASN80**	ND2	3.479	Weak
HIS708	N	**ALA57**	O	2.012	Very strong
HIS708	ND1	**ALA60**	O	1.695	Very strong
ASN709	N	**ALA56**	O	2.725	Strong
ASN709	OD1	**ASN80**	ND2	3.170	Weak
THR713	N	**ILE3**	O	2.547	Strong
LYS731	O	**TYR61**	N	1.588	Very strong
ASN733	N	**GLY54**	O	1.942	Very strong
ARG736	N	**ALA48**	O	3.187	Weak
TYR751	OH	**ARG66**	NH1	0.835	Very strong
HIS781	O	**TYR58**	OH	1.692	Very strong

[a] D-H..A dist.: Hydrogen (H) of donor (D)-acceptor (A) distance

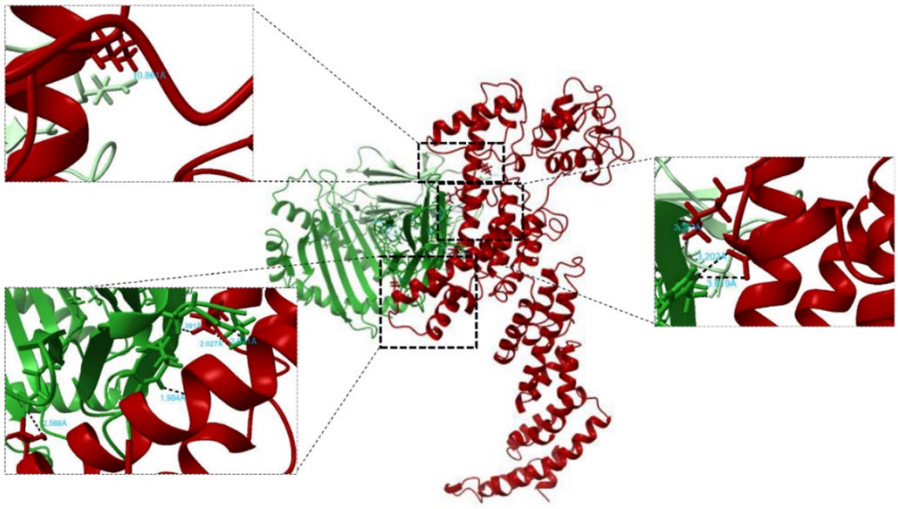

Figure S12. Analysis of molecular docking between HLA-A*11:01-anti-SARS-CoV-2 MEV in docked complex using UCSF ChimeraX [Vaccine construct in dark red, A chain of HLA-A*11:01 in dark green, β_2-microglubolin in light green; salt bridges and hydrogen bonds are displayed in cyan and black, respectively].

Table S10. Analysis of possible H-bonds and salt-bridges via molecular docking between HLA-A*11:01-anti-SARS-CoV-2-MEV in docked complex

Residue No.	Atom name	Residue No.	Atom name	D-H…A Distance (Å)	H-bond type according to (34)
HLA-A*11:01		MEV			
GLU74 (Hbond and salt bridge)	OE2	**LYS321**	NZ	0.861	Very strong
HIS192	ND1	**LYS348**	NZ	3.387	Weak
GLN218	NE2	**THR536**	OG1	2.588	Strong
GLN255	NE2	**LYS522**	O	2.671	Strong
ARG273	O	**ASN305**	ND2	1.391	Very strong
ARG273	NE	**LYS526**	O	1.984	Very strong
GLU275	OE1	**ASN305**	ND2	2.027	Very strong

[a] D-H..A dist.: Hydrogen (H) of donor (D)-acceptor (A) distance

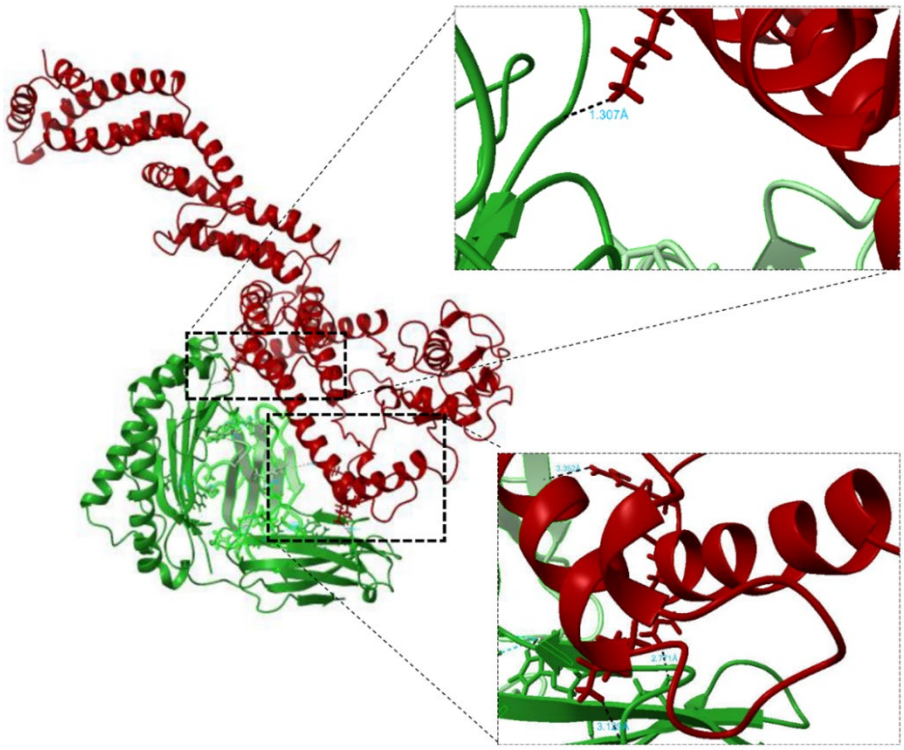

Figure S13. Analysis of molecular docking between HLA-A*68:01-anti-SARS-CoV-2 MEV in docked complex using UCSF Chimera X [Vaccine construct in dark red, A chain of HLA-A*68:01 in dark green, β_2-microglubolin in light green; salt bridges and hydrogen bonds are displayed in cyan and black, respectively].

Table S11. Analysis of possible H-bonds and salt-bridges via molecular docking between HLA-A*68:01-anti-SARS-CoV-2-MEV in docked complex

Residue No.	Atom name	Residue No.	Atom name	D-H…A Distance (Å)	H-bond type according to (34)
HLA-A*68:01		MEV			
ILE92	O	**ARG387**	NH2	3.352	Weak
SER92	O	**LYS298**	NZ	1.307	Very strong
THR200	OG1	**ARG386**	NH2	2.771	Strong
GLN224	O	**LYS330**	NZ	3.129	Weak

[a] D-H..A dist.: Hydrogen (H) of donor (D)-acceptor (A) distance

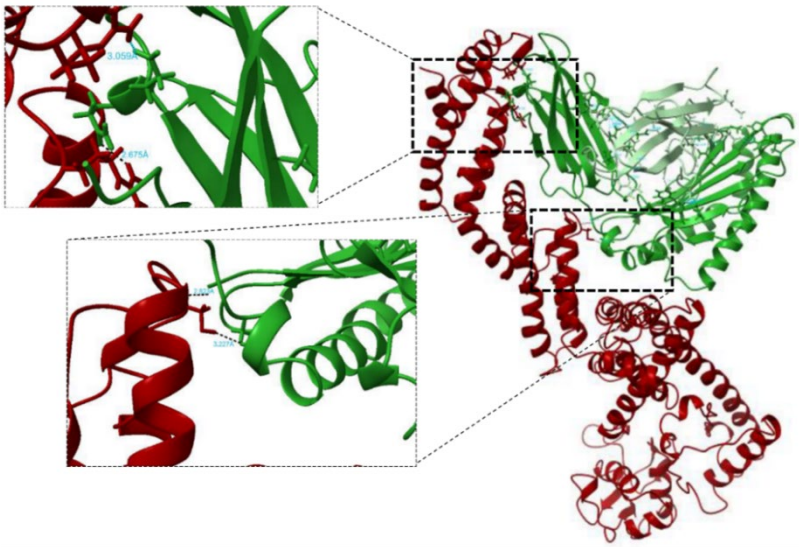

Figure S14. Analysis of molecular docking between HLA-B*35:01-anti-SARS-CoV-2 MEV in docked complex using UCSF ChimeraX [Vaccine construct in dark red, A chain of HLA-B*35:01 in dark green, β_2-microglubolin in light green; salt bridges and hydrogen bonds are displayed in cyan and black, respectively].

Table S12. Analysis of possible H-bonds and salt-bridges via molecular docking between HLA-B*35:01-anti-SARS-CoV-2-MEV in docked complex

Residue No.	Atom name	Residue No.	Atom name	D-H…A Distance (Å)	H-bond type according to (34)
HLA-B*35:01		**MEV**			
GLY1	N	**CYS199**	O	2.823	Strong
GLN180	OE1	**CYS199**	SG	3.227	Weak
GLN225	OE1	**ARG93**	NH1	2.675	Strong
GLU254 (Hbond and salt bridge)	OE1	**ARG38**	NH2	3.059	Strong

[a] D-H..A dist.: Hydrogen (H) of donor (D)-acceptor (A) distance

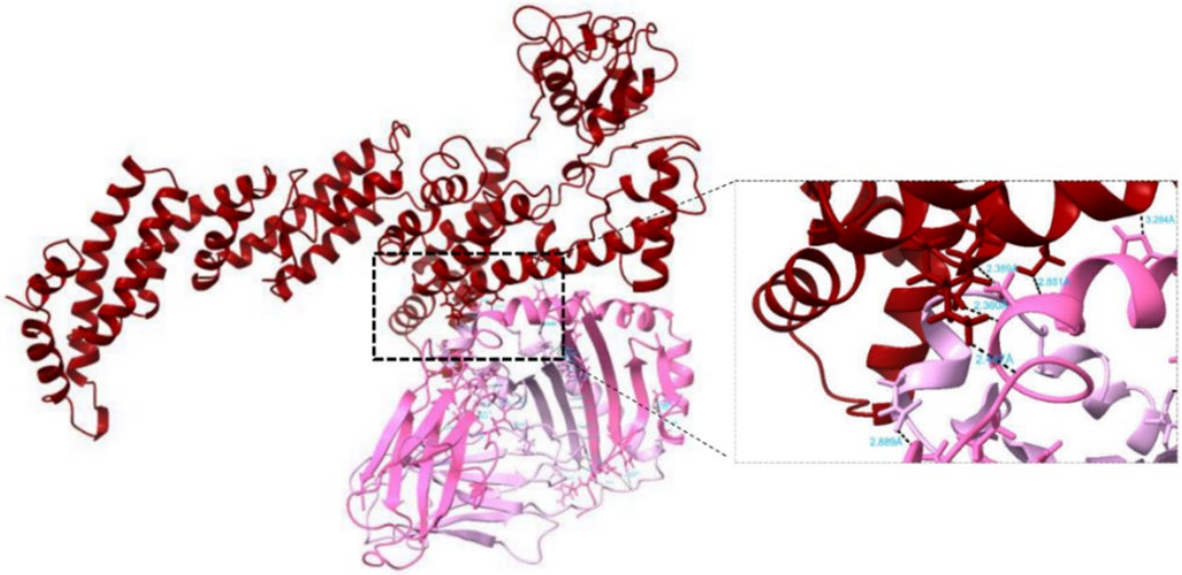

Figure S15. Analysis of molecular docking between HLA-DRB1*01:01-anti-SARS-CoV-2 MEV in docked complex using UCSF ChimeraX [Vaccine construct in dark red, A chain of HLA-DRB1*01:01 in dark pink, B chain of HLA-DRB1*01:01 in light pink; salt bridges and hydrogen bonds are displayed in cyan and black, respectively].

Table S13. Analysis of possible H-bonds and salt-bridges via molecular docking between HLA-DRB1*01:01-anti-SARS-CoV-2-MEV in docked complex

Residue No.	Atom name	Residue No.	Atom name	D-H…A Distance (Å)	H-bond type according to (34)
HLA-DRB1*01:01		**MEV**			
SER88	OG	**GLY304**	O	2.389	Very strong
SER88	O	**LYS307**	NZ	2.360	Very strong
SER88	N	**SER308**	OG	2.851	Strong
GLN92	O	**LYS298**	NZ	2.447	Very strong

[a] D-H..A dist.: Hydrogen (H) of donor (D)-acceptor (A) distance

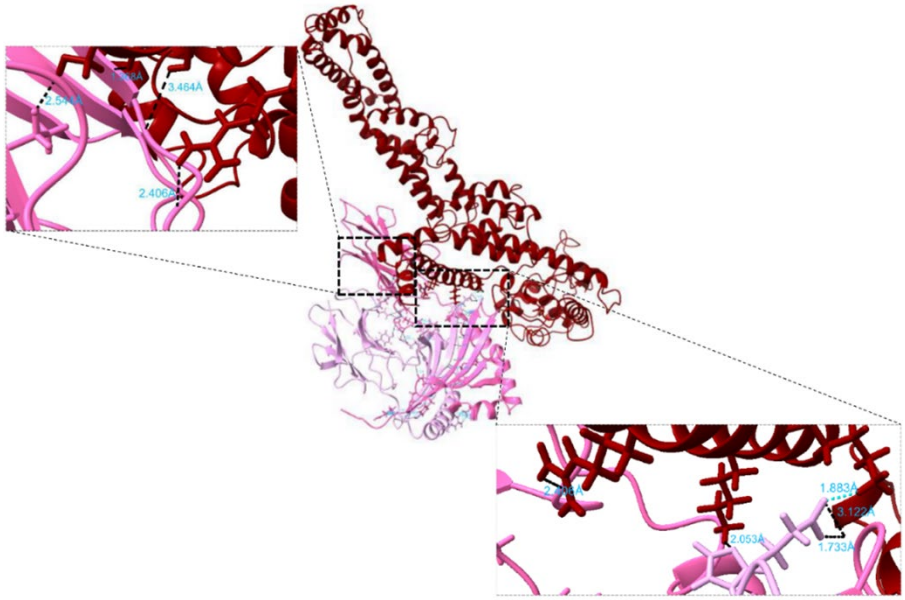

Figure S16. Analysis of molecular docking between HLA-DRB1*09:01-anti-SARS-CoV-2 MEV in docked complex using UCSF ChimeraX [Vaccine construct in dark red, A chain of HLA-DRB1*09:01 in dark pink, B chain of HLA-DRB1*01:01 in light pink; salt bridges and hydrogen bonds are displayed in cyan and black, respectively].

Table S14. Analysis of possible H-bonds and salt-bridges via molecular docking between HLA-DRB1*09:01-anti-SARS-CoV-2-MEV in docked complex

Residue No.	Atom name	Residue No.	Atom name	D-H…A Distance (Å)	H-bond type according to (34)[47]
HLA-DRB1*09:01		**MEV**			
GLU4 (Hbond and salt bridge)	OE2	**LYS518**	NZ	1.883	Very strong
HIS5	NE2	**LYS517**	NZ	2.053	Very strong
GLY125	O	**ARG524**	NH2	2.406	Very strong
ILE127	O	**SER564**	OG	3.464	Weak
VAL129	N	**ASP561**	OD2	1.368	Very strong
THR157	OG1	**SER563**	OG	2.544	Strong

[a] D-H..A dist.: Hydrogen (H) of donor (D)-acceptor (A) distance

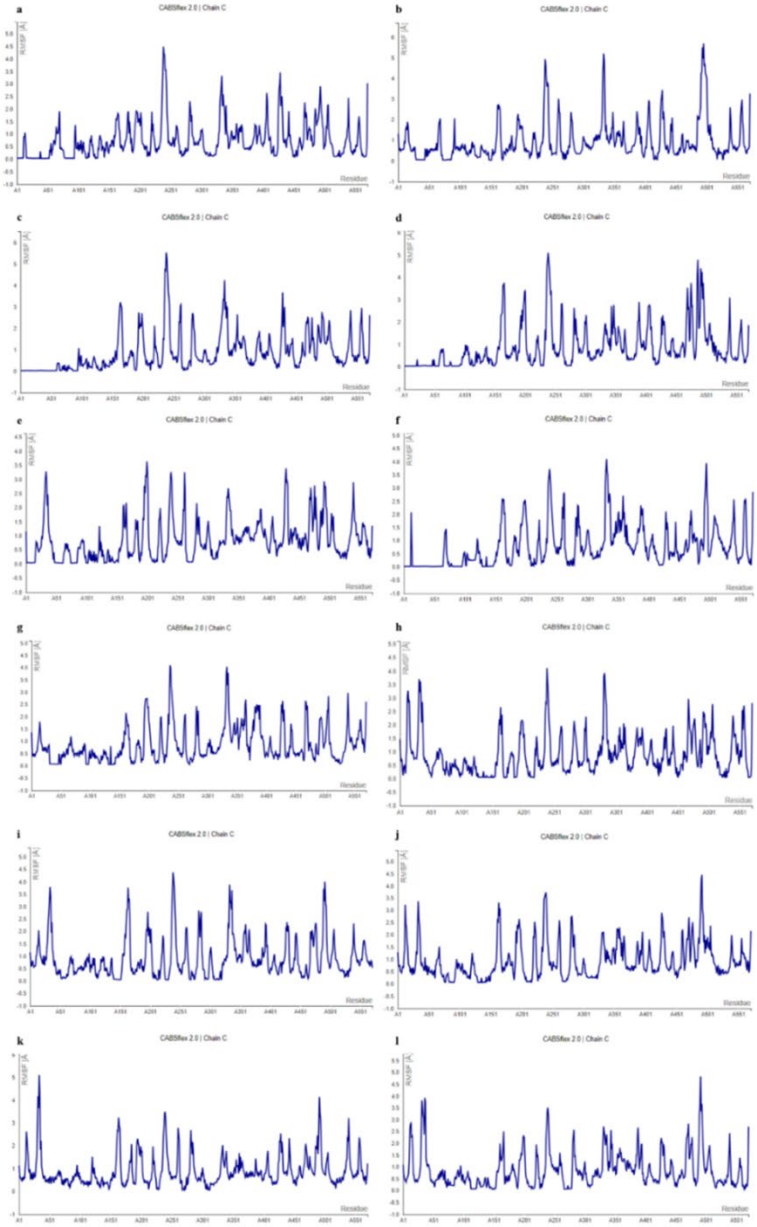

Figure S17. Analysis of RMSF fluctuation in the vaccine construct following the docking with **(a)** TLR2; **(b)** TLR3; **(c)** TLR4; **(d)** TLR5; **(e)** TLR7; **(f)** TLR8; **(g)** HLA-A*03:01; **(h)** HLA-A*11:01; **(i)** HLA-A*68:01; **(j)** HLA-B*35:01; **(k)** HLA-DRB1*01:01; **(l)** HLA-DRB1*09:01.

Table S15. Analysis the RMSF value of vaccine construct in complex with various immune receptors

Docked complex of MEV-TLRs:	Max. RMSF	Residue No.	Min. RMSF	Residue No.	Docked complex of MEV-MHC I/II:	Max. RMSF	Residue No.	Min. RMSF	Residue No.
TLR2	4.488	239	0.027	42, 46	**HLA-A*03:01**	4.096	237	0.051	143
TLR3	5.706	496	0.044	150	**HLA-A*11:01**	4.107	239	0.045	170
TLR4	5.539	239	0.019	49	**HLA-A*68:01**	4.38	239	0.049	230, 231
TLR5	5.098	239	0.034	79, 80	**HLA-B*35:01**	4.455	492	0.06	131

TLR7	3.638	200	0.028	75	**HLA-DRB1*01:01**	5.11	34	0.063	311
TLR8	4.101	332	0.02	94	**HLA-DRB1*09:01**	4.83	492	0.051	564

Table S16. Predicted eigenvalues of immune receptors with anti-SARS-CoV-2 MEV by iMODS server

TLRs-MEV complex	Eigenvalue	MHC I/II- MEV complex	Eigenvalue
TLR2	6.6325390e-06	**HLA-A*03:01**	1.740353e-05
TLR3	5.657387e-06	**HLA-A*11:01**	1.064208e-05
TLR4	5.021608e-06	**HLA-A*68:01**	1.177935e-05
TLR5	5.796432e-06	**HLA-B*35:01**	1.231407e-05
TLR7	6.139564e-06	**HLA-DRB1*01:01**	8.964068e-06
TLR8	7.832847e-06	**HLA-DRB1*09:01**	1.177296e-05

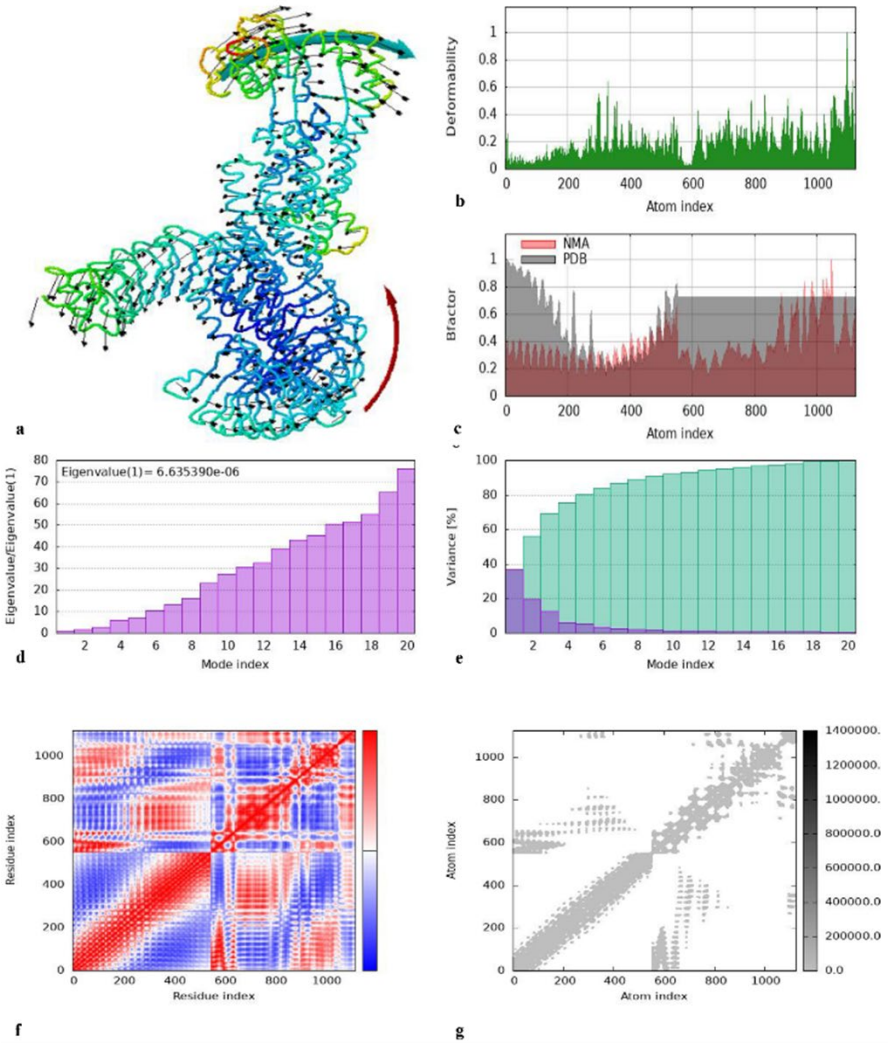

Figure S18. The dynamics simulation analysis of TLR2-MEV complex. **(a)** 3D structure of conformational dynamic motion; **(b)** deformability graph; **(c)** b-factor graph; **(d)** eigenvalue; **(e)** variance map (the green and colored columns show the cumulative and individual variances, respectively); **(f)** covariance matrix (The red, blue, and white colors show the correlated, un-correlated, and anti-correlated motions of each residue pairs, respectively); and **(g)** elastic network model (The darker grey dots show a more stiffness of connection between pair of atoms).

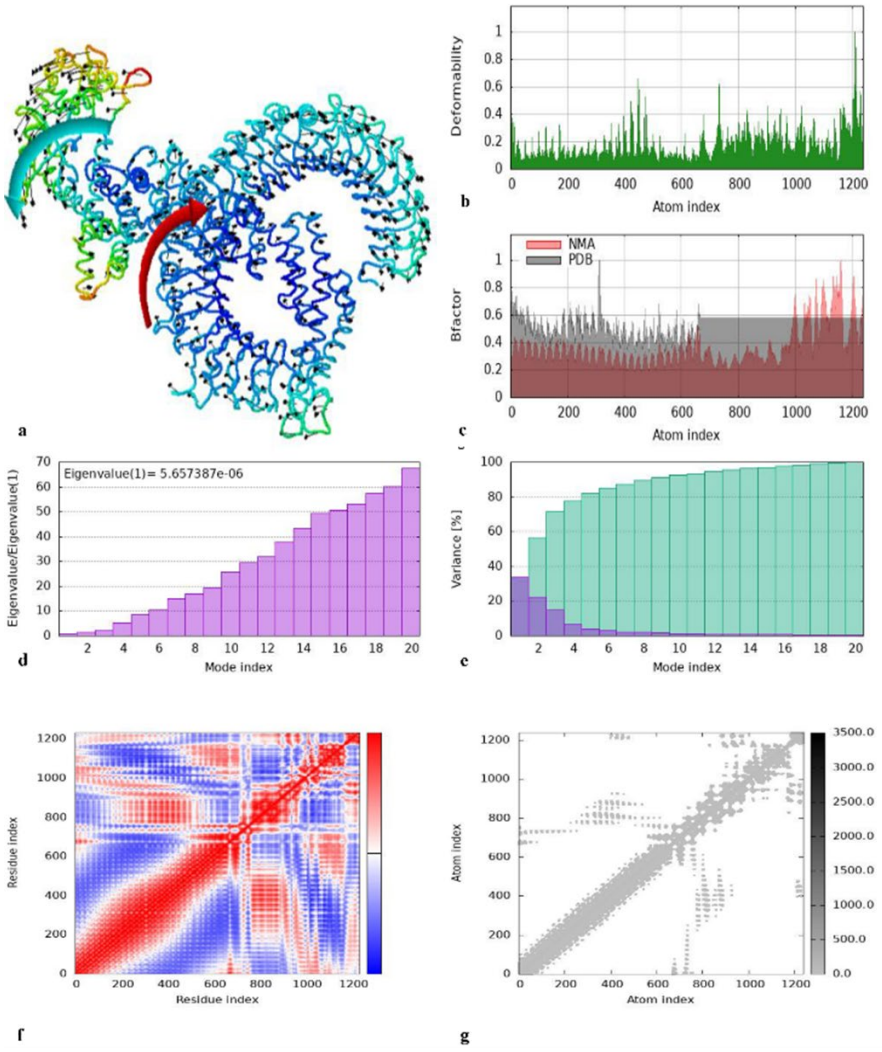

Figure S19. The dynamics simulation analysis of TLR3-MEV complex. **(a)** 3D structure of conformational dynamic motion; **(b)** deformability graph; **(c)** b-factor graph; **(d)** eigenvalue; **(e)** variance map (the green and colored columns show the cumulative and individual variances, respectively); **(f)** covariance matrix (The red, blue, and white colors show the correlated, un-correlated, and anti-correlated motions of each residue pairs, respectively); and **(g)** elastic network model (The darker grey dots show a more stiffness of connection between pair of atoms).

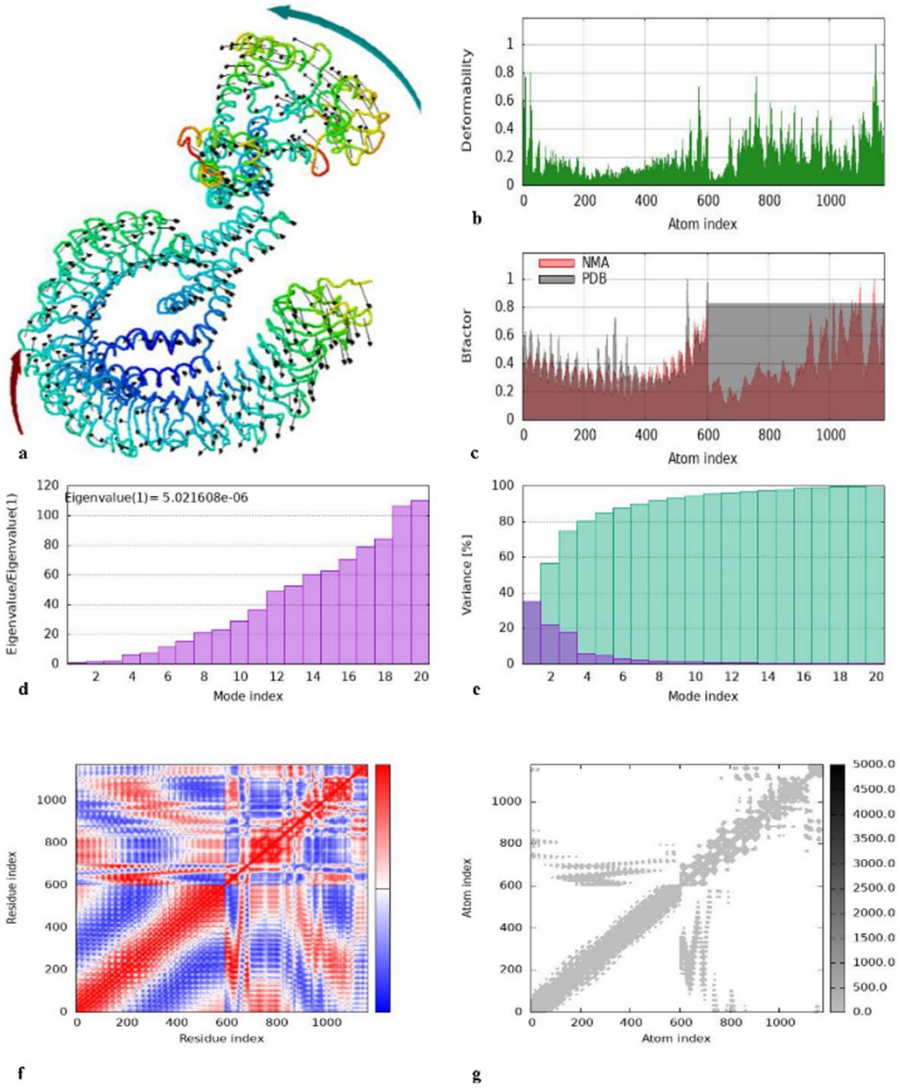

Figure S20. The dynamics simulation analysis of TLR4-MEV complex. **(a)** 3D structure of conformational dynamic motion; **(b)** deformability graph; **(c)** b-factor graph; **(d)** eigenvalue; **(e)** variance map (the green and colored columns show the cumulative and individual variances, respectively); **(f)** covariance matrix (The red, blue, and white colors show the correlated, un-correlated, and anti-correlated motions of each residue pairs, respectively); and **(g)** elastic network model (The darker grey dots show a more stiffness of connection between pair of atoms).

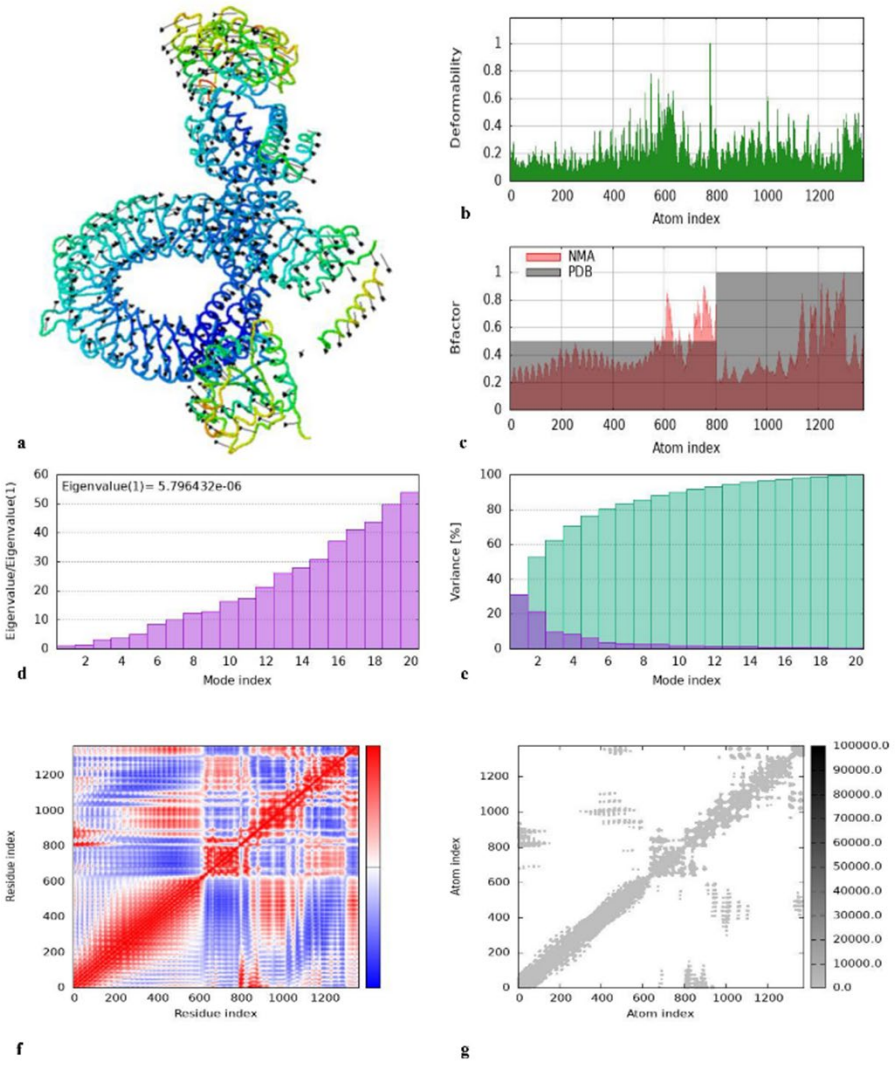

Figure S21. The dynamics simulation analysis of TLR5-MEV complex. **(a)** 3D structure of conformational dynamic motion; **(b)** deformability graph; **(c)** b-factor graph; **(d)** eigenvalue; **(e)** variance map (the green and colored columns show the cumulative and individual variances, respectively); **(f)** covariance matrix (The red, blue, and white colors show the correlated, un-correlated, and anti-correlated motions of each residue pairs, respectively); and **(g)** elastic network model (The darker grey dots show a more stiffness of connection between pair of atoms).

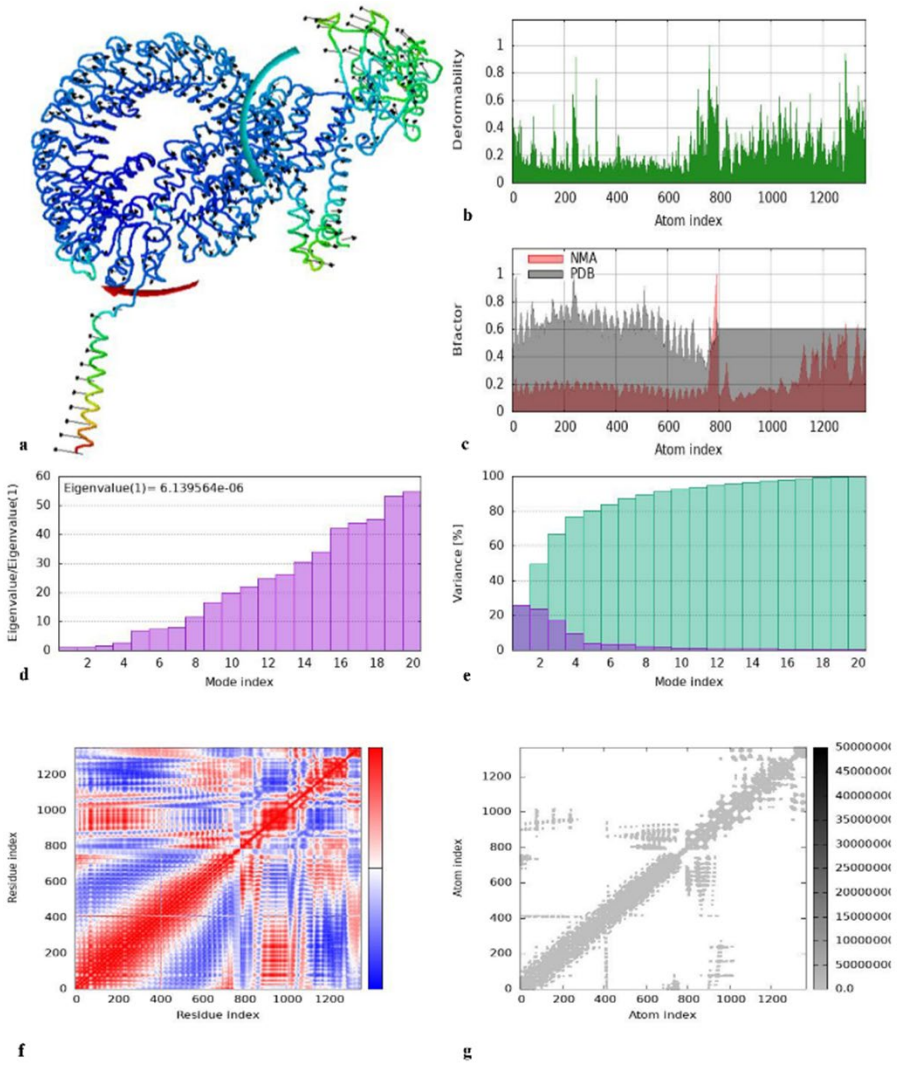

Figure S22. The dynamics simulation analysis of TLR7-MEV complex. **(a)** 3D structure of conformational dynamic motion; **(b)** deformability graph; **(c)** b-factor graph; **(d)** eigenvalue; **(e)** variance map (the green and colored columns show the cumulative and individual variances, respectively); **(f)** covariance matrix (The red, blue, and white colors show the correlated, un-correlated, and anti-correlated motions of each residue pairs, respectively); and **(g)** elastic network model (The darker grey dots show a more stiffness of connection between pair of atoms).

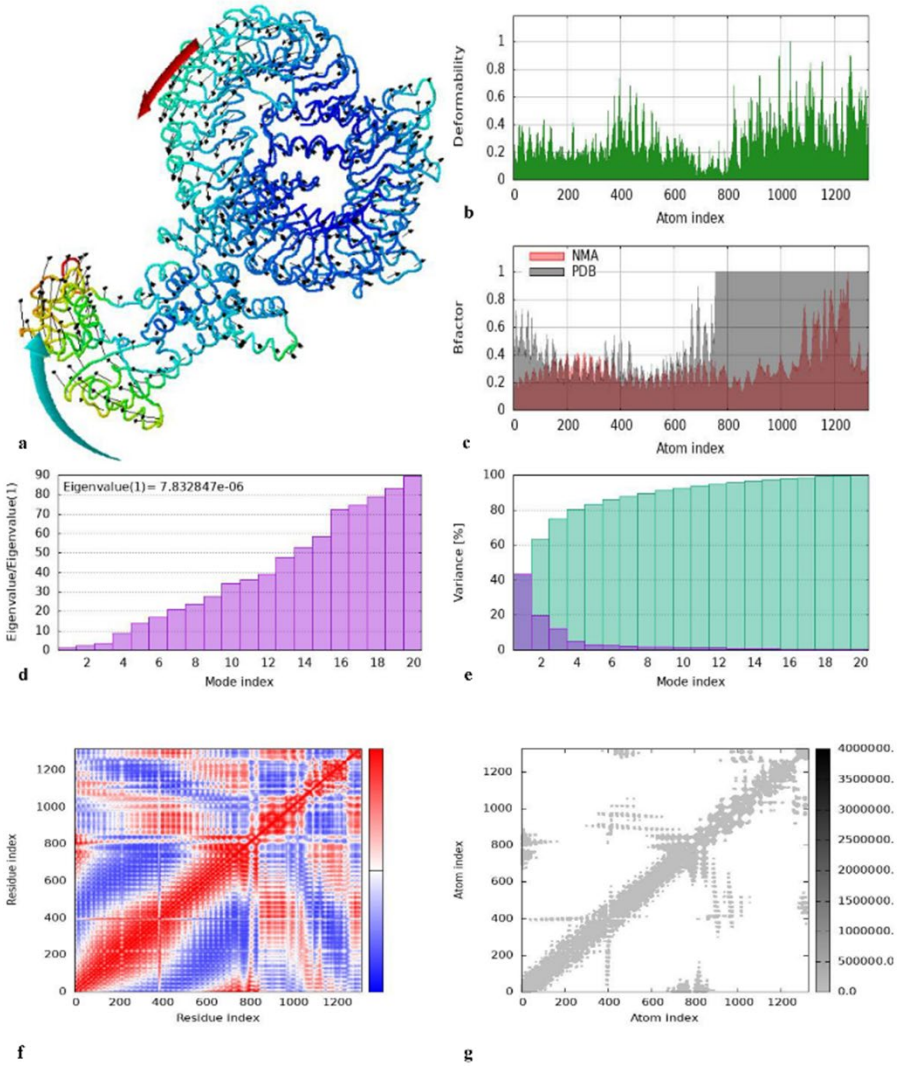

Figure S23. The dynamics simulation analysis of TLR8-MEV complex. **(a)** 3D structure of conformational dynamic motion; **(b)** deformability graph; **(c)** b-factor graph; **(d)** eigenvalue; **(e)** variance map (the green and colored columns show the cumulative and individual variances, respectively); **(f)** covariance matrix (The red, blue, and white colors show the correlated, un-correlated, and anti-correlated motions of each residue pairs, respectively); and **(g)** elastic network model (The darker grey dots show a more stiffness of connection between pair of atoms).

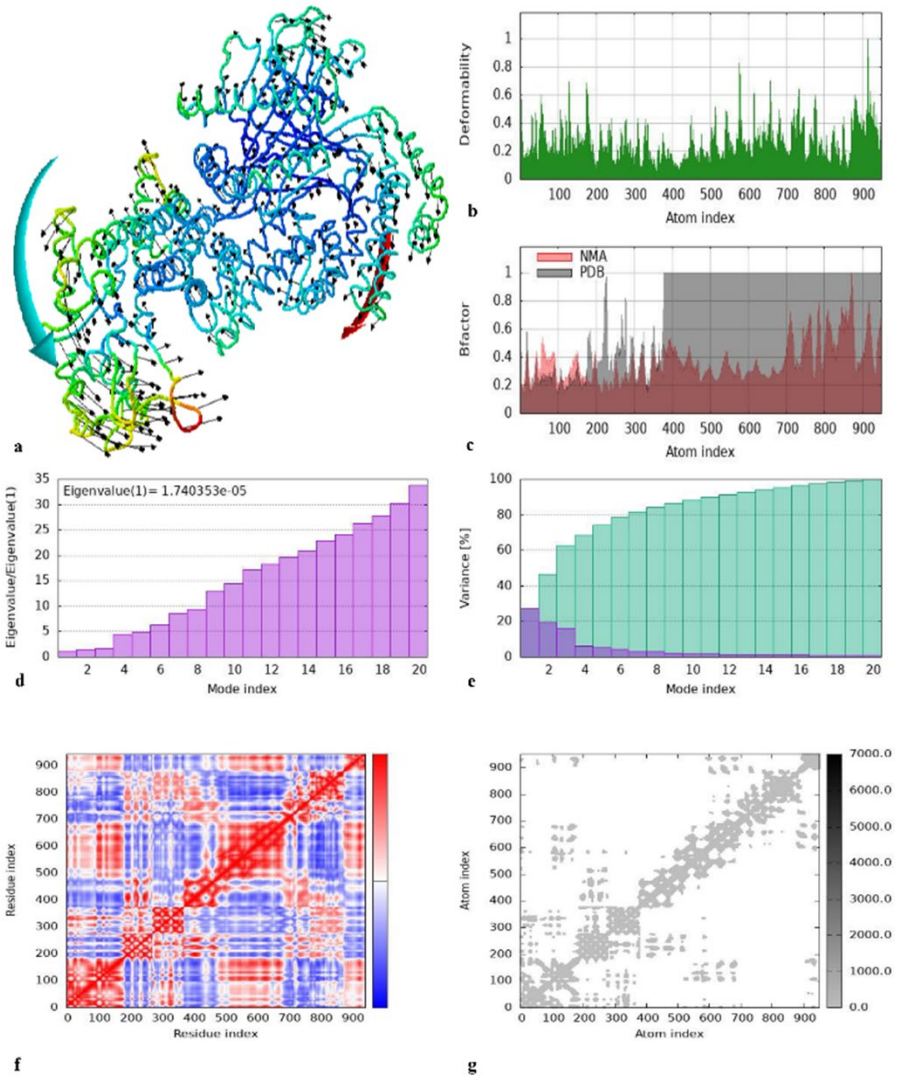

Figure S24. The dynamics simulation analysis of HLA-A*03:01-MEV complex. **(a)** 3D structure of conformational dynamic motion; **(b)** deformability graph; **(c)** b-factor graph; **(d)** eigenvalue; **(e)** variance map (the green and colored columns show the cumulative and individual variances, respectively); **(f)** covariance matrix (The red, blue, and white colors show the correlated, un-correlated, and anti-correlated motions of each residue pairs, respectively); and **(g)** elastic network model (The darker grey dots show a more stiffness of connection between pair of atoms).

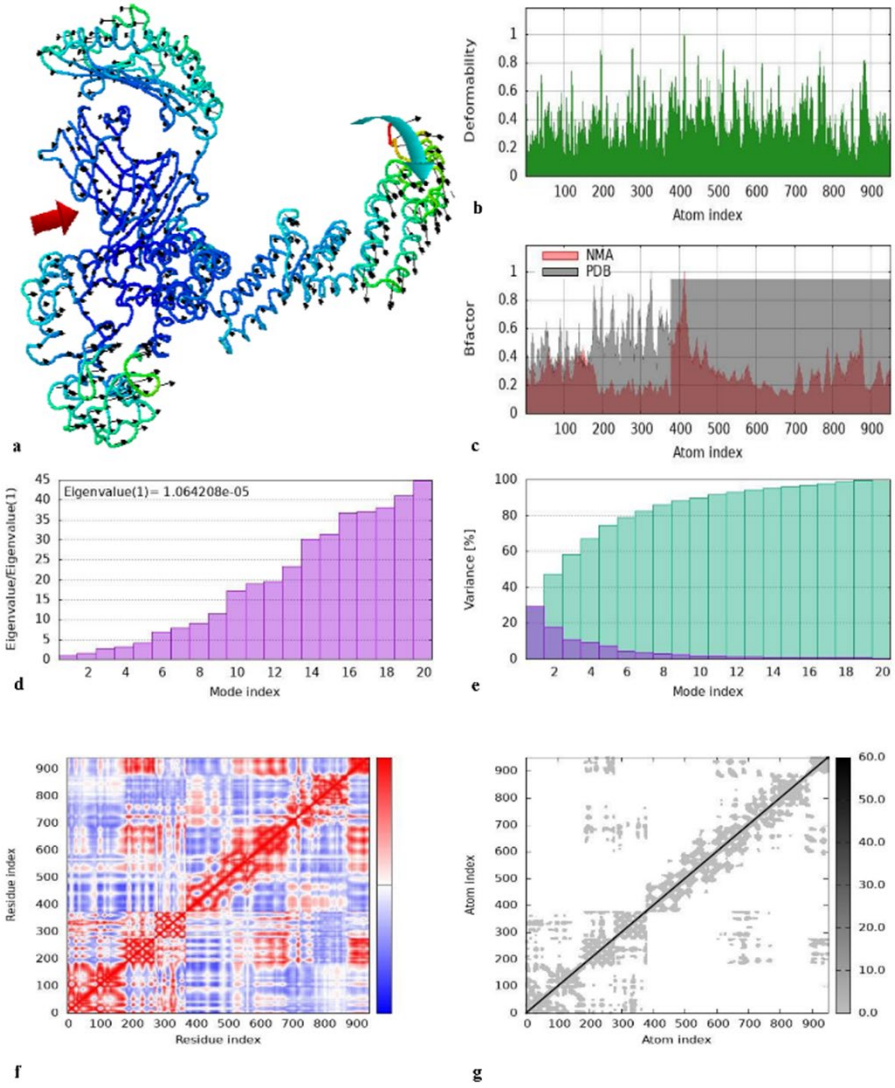

Figure S25. The dynamics simulation analysis of HLA-A*11:01-MEV complex. **(a)** 3D structure of conformational dynamic motion; **(b)** deformability graph; **(c)** b-factor graph; **(d)** eigenvalue; **(e)** variance map (the green and colored columns show the cumulative and individual variances, respectively); **(f)** covariance matrix (The red, blue, and white colors show the correlated, un-correlated, and anti-correlated motions of each residue pairs, respectively); and **(g)** elastic network model (The darker grey dots show a more stiffness of connection between pair of atoms).

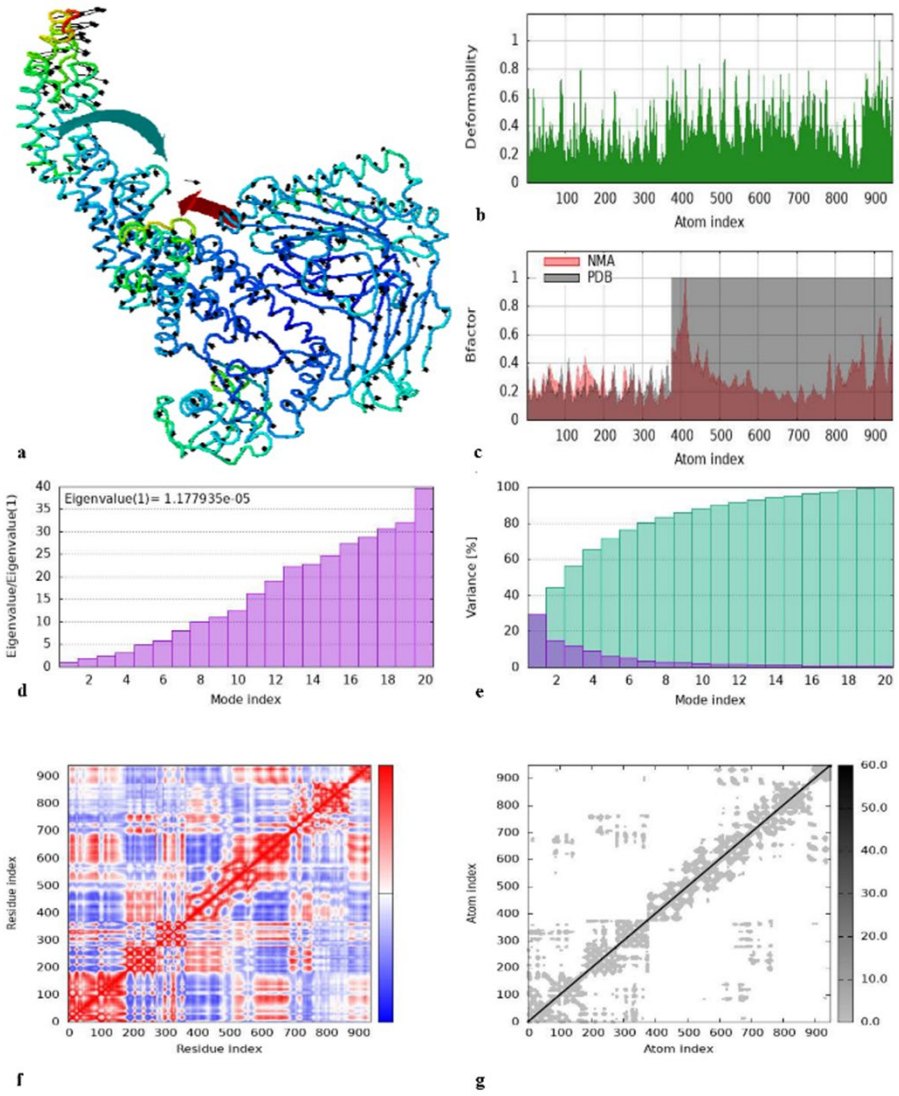

Figure S26. The dynamics simulation analysis of HLA-A*68:01-MEV complex. **(a)** 3D structure of conformational dynamic motion; **(b)** deformability graph; **(c)** b-factor graph; **(d)** eigenvalue; **(e)** variance map (the green and colored columns show the cumulative and individual variances, respectively); **(f)** covariance matrix (The red, blue, and white colors show the correlated, un-correlated, and anti-correlated motions of each residue pairs, respectively); and **(g)** elastic network model (The darker grey dots show a more stiffness of connection between pair of atoms).

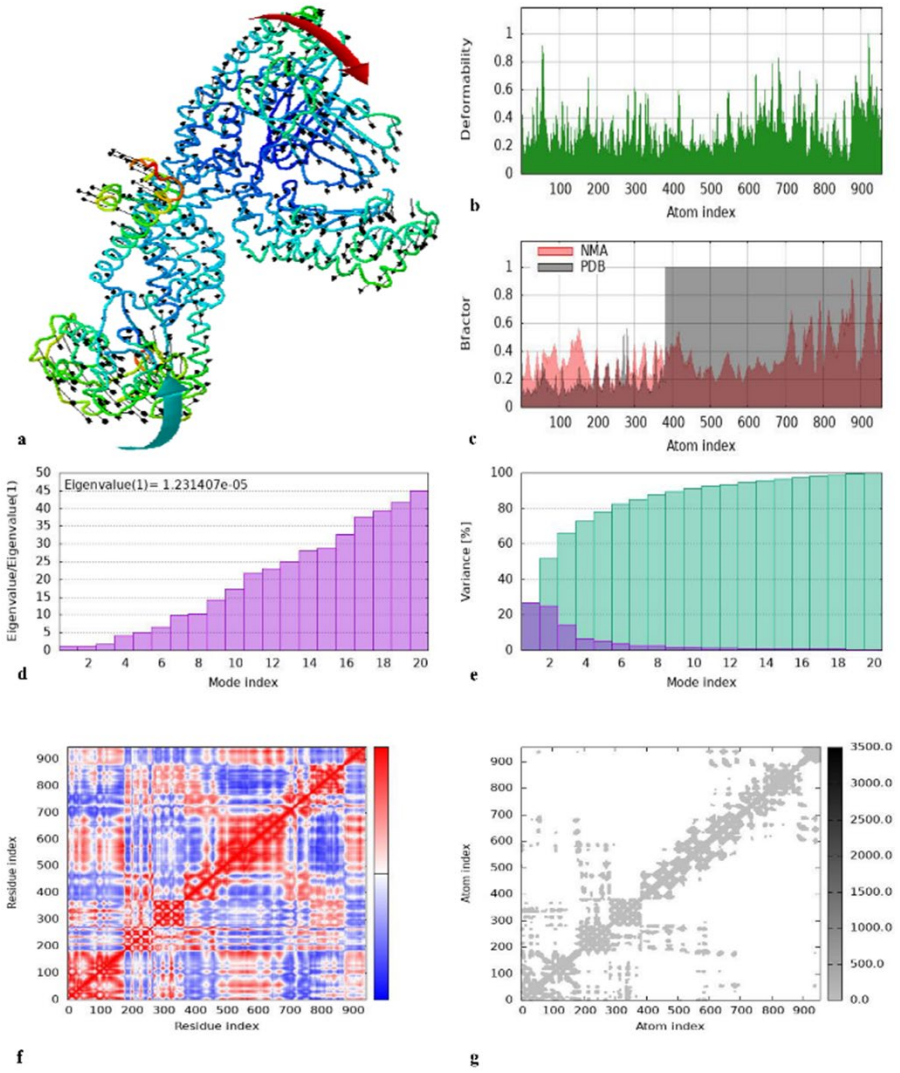

Figure S27. The dynamics simulation analysis of HLA-B*35:01-MEV complex. **(a)** 3D structure of conformational dynamic motion; **(b)** deformability graph; **(c)** b-factor graph; **(d)** eigenvalue; **(e)** variance map (the green and colored columns show the cumulative and individual variances, respectively); **(f)** covariance matrix (The red, blue, and white colors show the correlated, un-correlated, and anti-correlated motions of each residue pairs, respectively); and **(g)** elastic network model (The darker grey dots show a more stiffness of connection between pair of atoms).

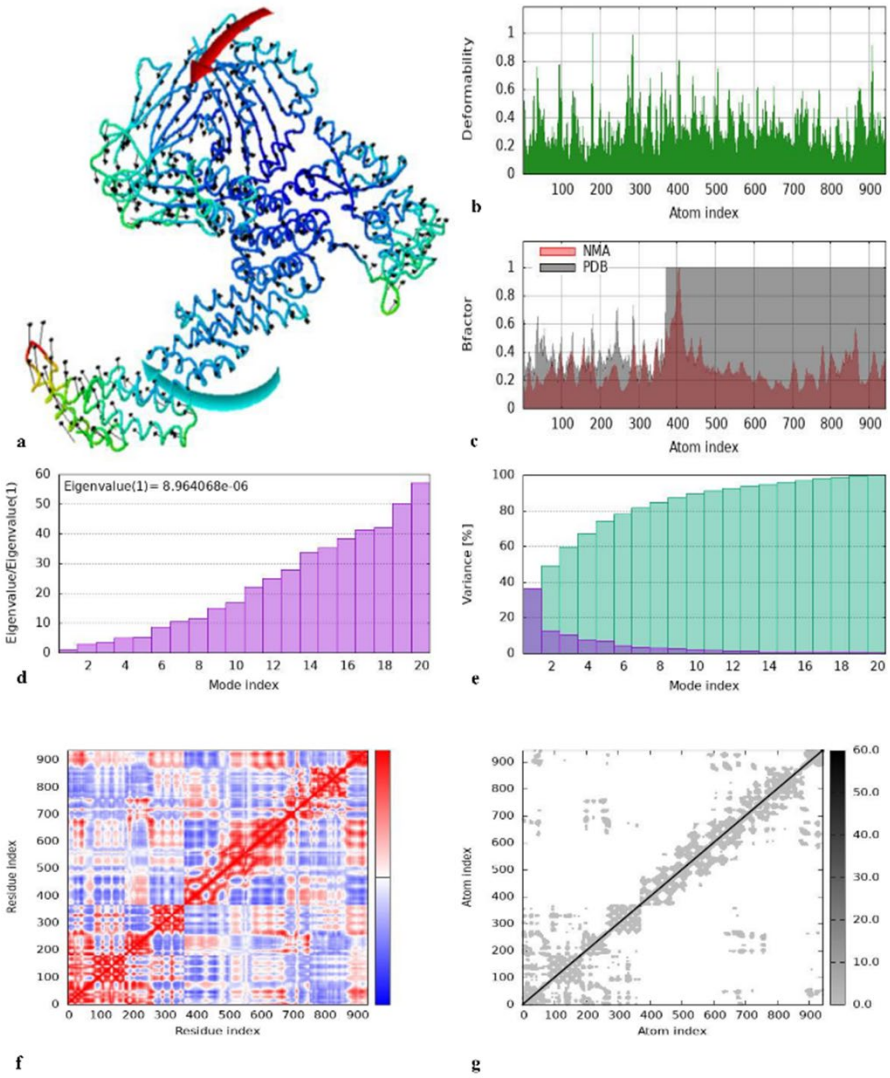

Figure S28. The dynamics simulation analysis of HLA-DRB1*01:01-MEV complex. **(a)** 3D structure of conformational dynamic motion; **(b)** deformability graph; **(c)** b-factor graph; **(d)** eigenvalue; **(e)** variance map (the green and colored columns show the cumulative and individual variances, respectively); **(f)** covariance matrix (The red, blue, and white colors show the correlated, un-correlated, and anti-correlated motions of each residue pairs, respectively); and **(g)** elastic network model (The darker grey dots show a more stiffness of connection between pair of atoms).

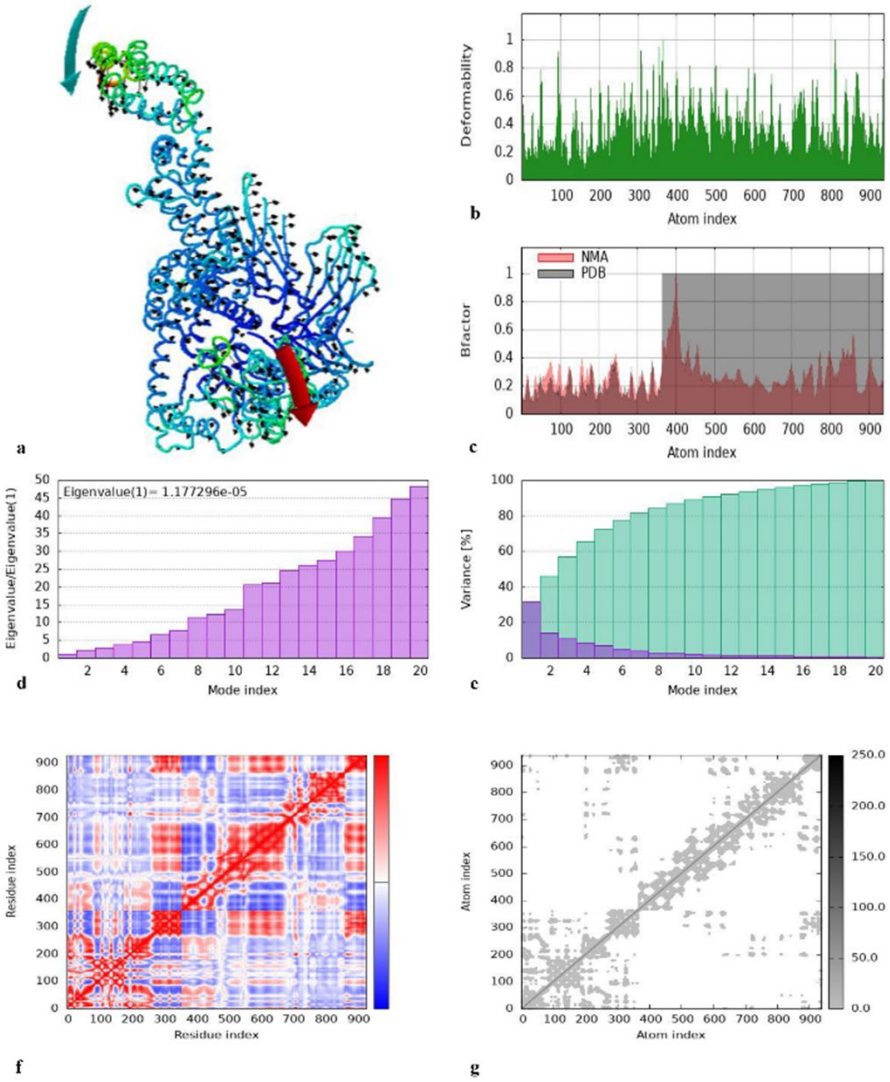

Figure S29. The dynamics simulation analysis of HLA-DRB1*09:01-MEV complex. **(a)** 3D structure of conformational dynamic motion; **(b)** deformability graph; **(c)** b-factor graph; **(d)** eigenvalue; **(e)** variance map (the green and colored columns show the cumulative and individual variances, respectively); **(f)** covariance matrix (The red, blue, and white colors show the correlated, un-correlated, and anti-correlated motions of each residue pairs, respectively); and **(g)** elastic network model (The darker grey dots show a more stiffness of connection between pair of atoms).

Table S17. Analysis of possible H-bonds and salt-bridges via molecular docking between ACE2-anti-SARS-CoV-2-MEV in docked complex

Residue No.	Atom name	Residue No.	Atom name	D-H…A Distance (Å)	H-bond type according to (34)[47]
ACE2		**MEV**			
ASN137	ND2	**ASP469**	O	3.809	Weak
GLN139	NE2	**ASP469**	OD2	3.180	Weak
GLU140	OE1	**ALA477**	N	4.891	Weak
CYS141	O	**ASP481**	N	3.890	Weak
LEU143	O	**LYS467**	NZ	3.899	Weak

GLN145 (Hbond and salt bridge)	OE2	**LYS429**	NZ	3.704	Weak
PRO146	O	**THR438**	N	4.675	Weak
GLY147	O	**LEU437**	N	3.530	Weak
	O	**THR438**	N	3.997	Weak
ASN149	N	**LEU433**	O	4.138	Weak
	N	**ASP481**	OD1	4.197	Weak
	ND2	**ASN432**	OD1	4.346	Weak
	ND2	**LEU433**	O	3.688	Weak
	O	**LYS441**	NZ	4.134	Weak
GLU150	O	**LYS441**	N	3.272	Weak
	N	**LEU433**	O	4.509	Weak
	O	**TYR442**	N	5.152	Weak
	O	**LYS450**	NZ	4.896	Weak
	OE2 (Hbond and salt bridge)	**LYS450**	NZ	3.817	Weak
	N	**ASP481**	OD1	4.977	Weak
ILE151	N	**ALA480**	O	4.731	Weak
	O	**ASN440**	N	4.843	Weak
	O	**ASN449**	ND2	4.289	Weak
	O	**LYS450**	NZ	4.832	Weak
ALA153	O	**GLN444**	NE2	4.220	Weak
ASN154	N	**LYS435**	O	5.032	Weak
	ND2	**SER443**	O	2.169	Strong
	O	**LEU445**	N	3.981	Weak
LEU156	N	**GLU447**	OE2	3.355	Weak
ASP157	N	**GLU447**	OE2	3.558	Weak
GLU160	OE2 (Hbond and salt bridge)	**LYS450**	NZ	2.860	Strong
	OE1	**ALA480**	N	4.730	Weak
ASR161	NH1	**LEU437**	O	4.126	Weak
LEU162	O	**LYS479**	NZ	4.010	Weak
SER167	OG	**LYS479**	NZ	0.714	Very strong
HIS265	O	**LYS441**	NZ	5.151	Weak
PHE274	O	**LYS441**	NZ	5.017	Weak
THR276	O	**ARG365**	NH1	4.453	Weak
	O	**ARG365**	NH2	2.996	Strong
ASN277	O	**ARG365**	NH1	4.481	Weak
SER280	OG	**ASN440**	O	5.273	Weak
GLN287	NE2	**GLN391**	OE1	3.888	Weak
	O	**GLN391**	NE2	5.111	Weak
ASN290	O	**ARG378**	NH1	3.669	Weak
ASP292	OD1	**LYS368**	N	3.446	Weak
	OD2	**LYS368**	N	4.590	Weak
	OD2	**SER374**	OG	4.510	Weak
	O	**LYS375**	N	2.325	Very strong
VAL293	N	**LYS366**	O	4.827	Weak
THR294	N	**LYS366**	O	4.370	Weak
	O	**THR337**	N	2.965	Strong
	O	**THR337**	OG1	3.639	Weak
ASP295	O	**TYR335**	N	3.924	Weak
	O	**GLN336**	N	3.850	Weak
	O	**THR337**	N	3.914	Weak
ALA296	N	**GLU372**	OE1	5.098	Weak
	P	**LYS376**	NZ	5.037	Weak
MET297	N	**SER369**	O	4.679	Weak
VAL298	N	**SER369**	O	4.279	Weak
ASP299	OD1	**VAL342**	N	4.460	Weak
GLN300	NE2	**LYS330**	O	5.088	Weak
ALA301	N	**THR337**	O	2.819	Strong
TRP302	N	**THR337**	O	4.315	Weak
	NE1	**LYS332**	O	4.813	Weak
ARG306	NH1	**LYS332**	O	5.135	Weak
ASP335	O	**LYS410**	NZ	4.441	Weak
ASN338	ND2	**LYS409**	O	2.149	Very strong

	ND2	**LUE486**	O	2.911	Strong
	ND2	**HIS488**	O	4.085	Weak
LYS341	NZ	**GLY405**	O	5.547	Weak
	NZ	**LEU486**	O	3.790	Weak
CYS344	N	**LYS429**	O	4.466	Weak
LEU359	O	**LYS428**	NZ	5.035	Weak
VAL364	O	**THR337**	OG1	3.956	Weak
	O	**SER369**	N	0.905	Very strong
	O	**LYS427**	NZ	5.013	Weak
MET366	N	**SER369**	O	4.939	Weak
ASP368 (Hbond and salt bridge)	OD1	**LYS366**	NZ	2.200	Very strong
	OD1	**LYS368**	NZ	1.850	Very strong
	OD1	**LYS428**	NZ	4.569	Weak
	OD2	**LYS368**	NZ	2.611	Very strong
	OD2	**LYS428**	NZ	4.528	Weak
PHE369	N	**LYS367**	O	2.224	Very strong
LEU370	N	**LYS367**	O	3.977	Weak
THR371	OG1	**LYS366**	NZ	1.488	Very strong
SER409	O	**LYS367**	NZ	4.709	Weak
THR414	O	**LYS367**	NZ	4.249	Weak
GLY422	O	**LYS376**	NZ	4.166	Weak
SER425	OG	**LYS380**	NZ	4.617	Weak
ASP427 (Hbond and salt bridge)	OD2	**LYS380**	NZ	4.576	Weak
GLN429	O	**GLN379**	NE2	4.949	Weak
LYS441	NZ	**ARG365**	O	3.854	Weak

[a] D-H..A dist.: Hydrogen (H) of donor (D)-acceptor (A) distance

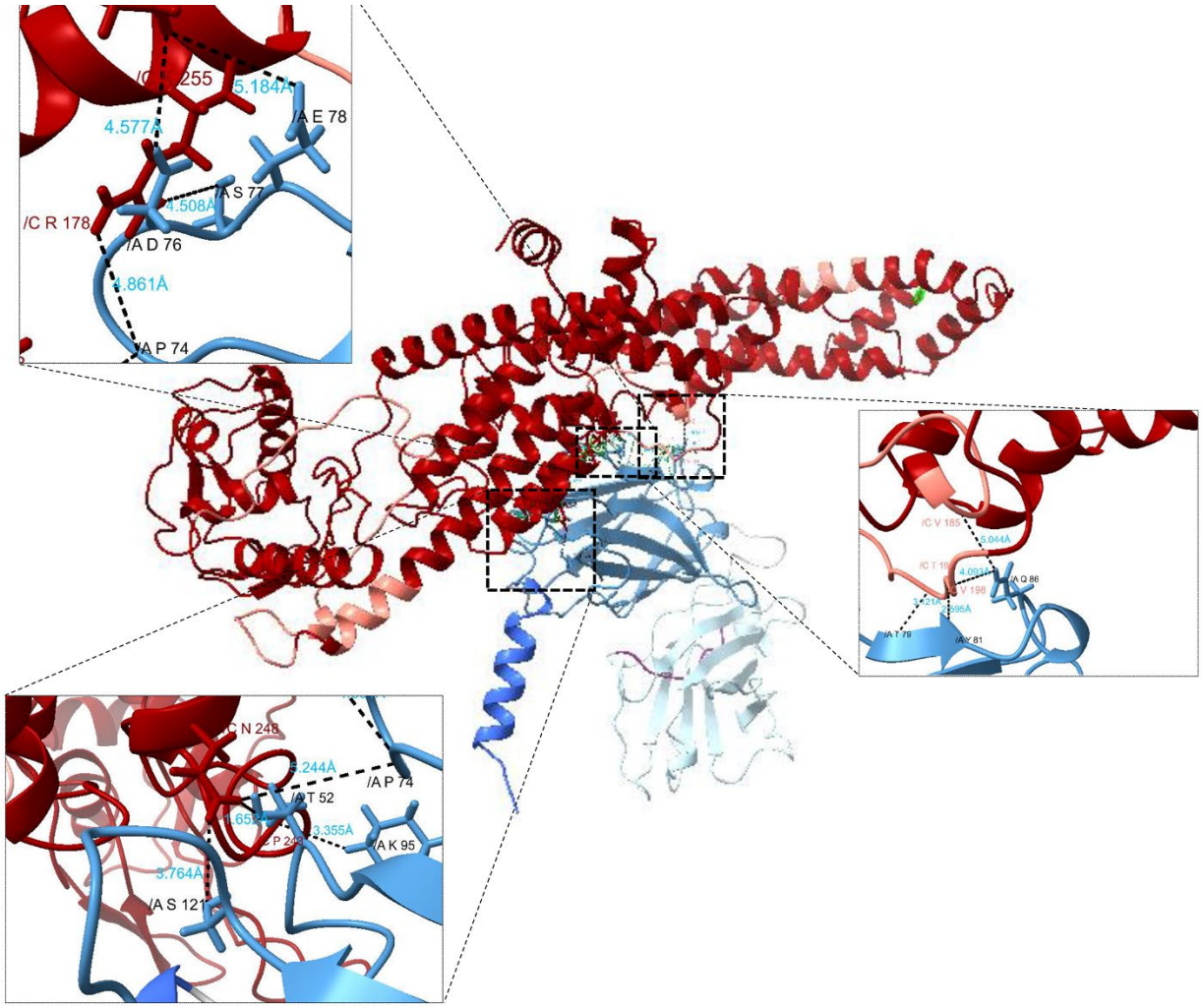

Figure S30. Analysis of molecular docking between scFv-anti-SARS-CoV-2 MEV in docked complex using UCSF ChimeraX [Vaccine construct in dark red, scFv in blue; salt bridges and hydrogen bonds are displayed in cyan and black, respectively].

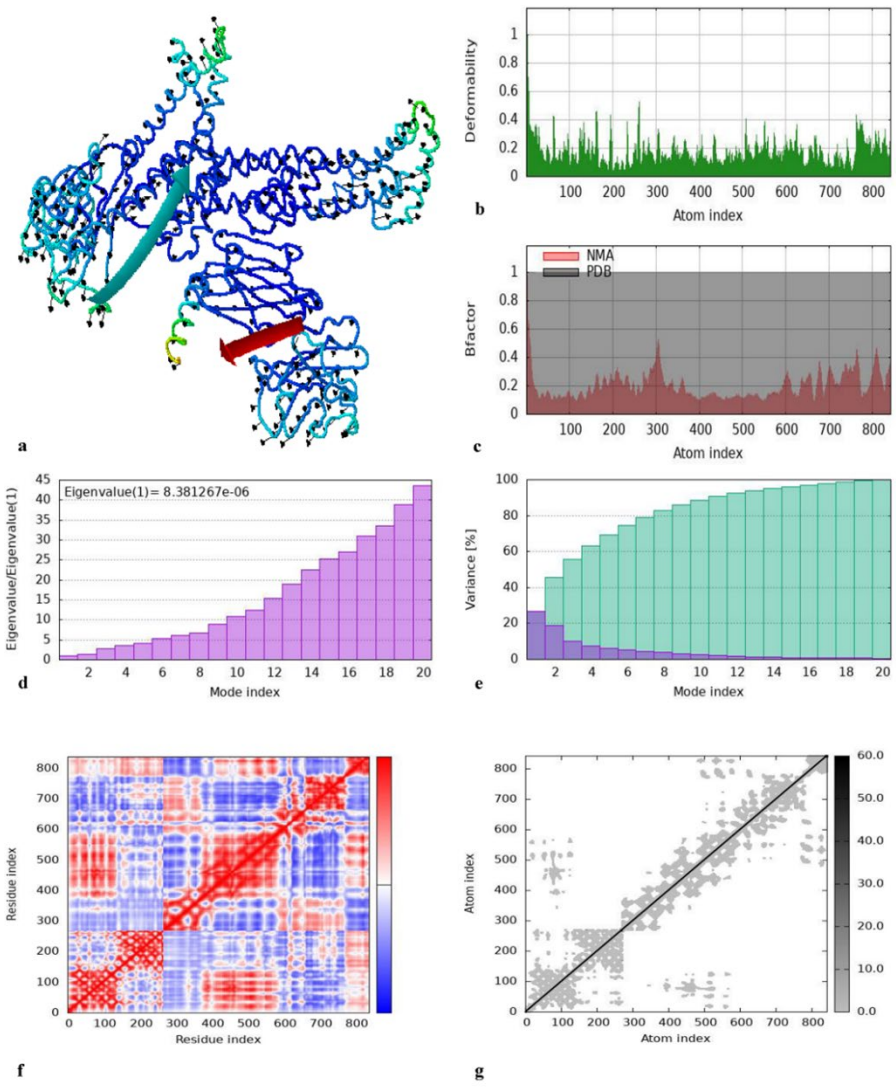

Figure S31. The dynamics simulation analysis of scFv-MEV complex. **(a)** 3D structure of conformational dynamic motion; **(b)** deformability graph; **(c)** b-factor graph; **(d)** eigenvalue; **(e)** variance map (the green and colored columns show the cumulative and individual variances, respectively); **(f)** covariance matrix (The red, blue, and white colors show the correlated, un-correlated, and anti-correlated motions of each residue pairs, respectively); and **(g)** elastic network model (The darker grey dots show a more stiffness of connection between pair of atoms).

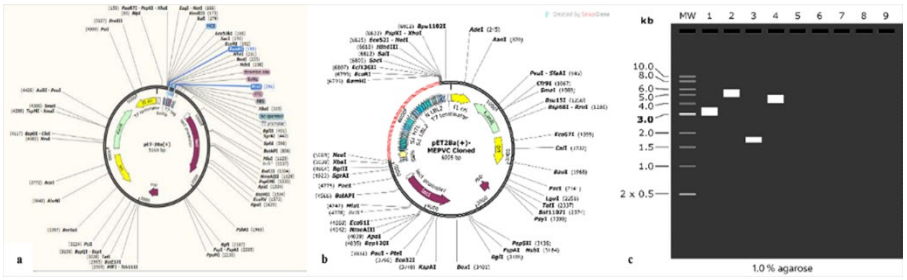

Figure S1. In-silico cloning of anti-SARS-CoV-2 MEV by SnapGene®. **(a)** pET28a(+) vector with highlighted Res for cloning; **(b)** cloned pET28a(+)-anti-SARS-CoV-2 MEV (the construct was shown in red); **(c)** simulation of agarose electrophoresis: **1:** 1kb DNA ladder; **2:** pET28a(+); **3:** designed MEV; **4:** pET28a(+)-anti-SARS-CoV-2-MEV (~6995bp).

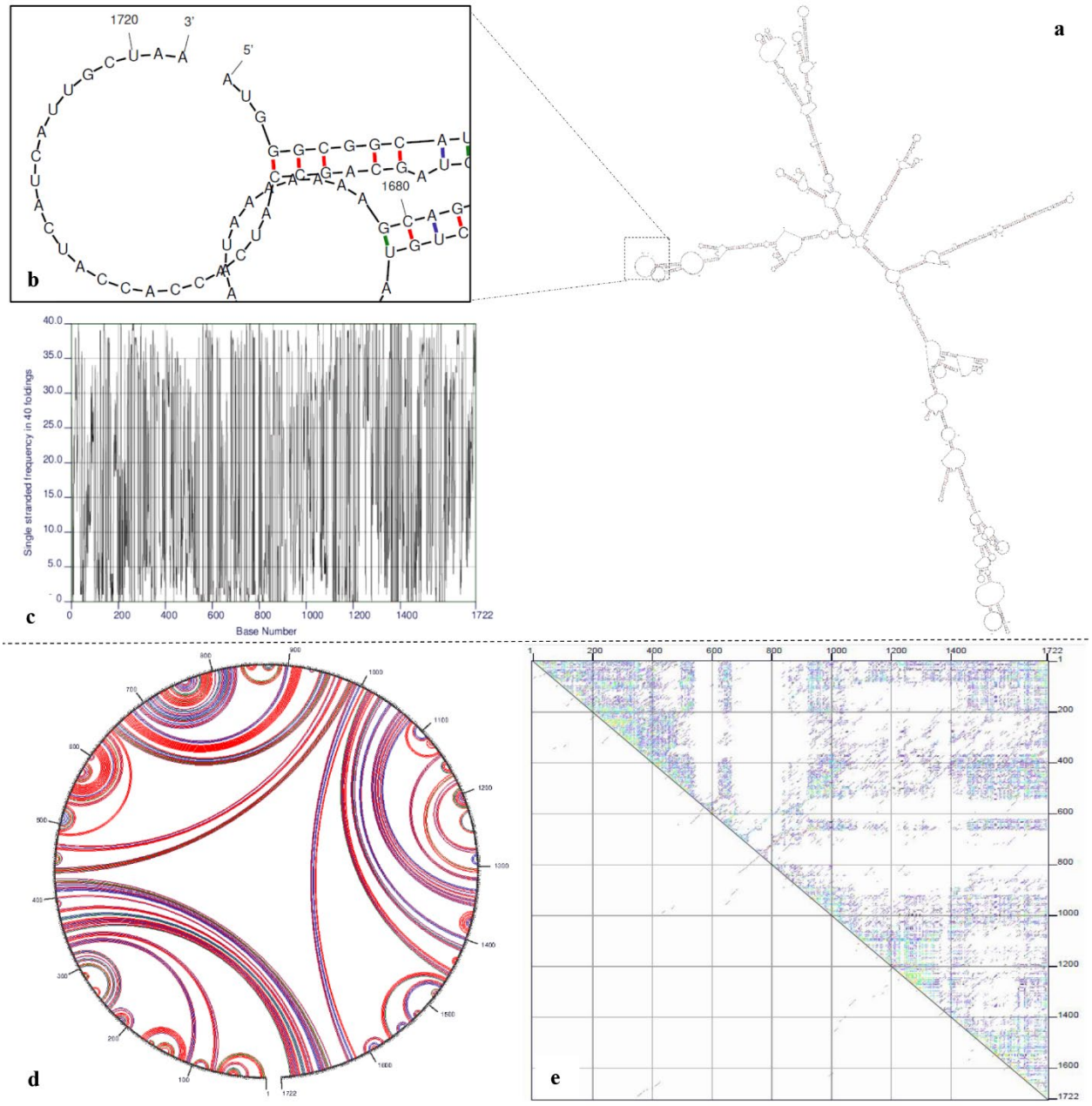

Figure S33. Analysis of mRNA structure of MEV. **(a)** Full mRNA secondary structure; **(b)** The 5' and 3' ends of mRNA structure showed no hairpin or pseudoknots; **(c)** Frequency of single-stranded (ss) structure in MEV sequence; graphical view **(d)** and dot plot **(e)** representation of mRNA structure. In part d, G-C, A-U, G-U, and other arcs are shown in red, blue, green, and yellow, respectively.

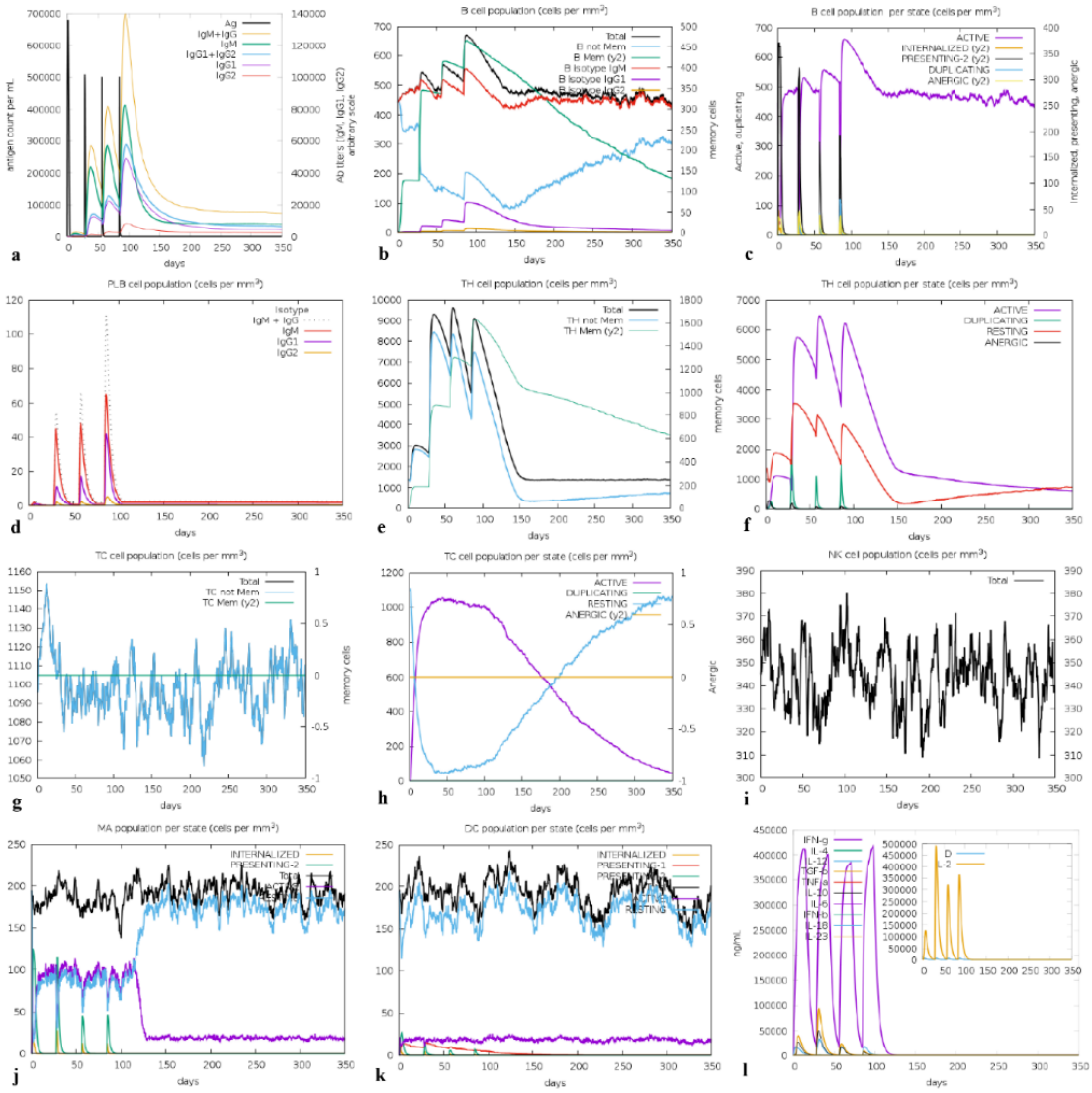

Figure S34. The immune simulation results of designed anti-SARS-CoV-2 vaccine using c-ImmSim during the four vaccinations with 28 days intervals. **(a)** the positive change in immunoglobulins amounts; **(b-c)** B-cell responses to vaccinations; **(e-f)** variation in T_H population and state during vaccination; **(g-h)** variation in T_C population and state during vaccination; **(i)** variation in NK cell population; **(j-k)** the positive changes in population of macrophages (MA) and dendritic cell (DCs), as the APCs, during the vaccination; **(l)** the cytokine- and interleukin-inducing ability of the vaccine construct.